Neurobiology of Disease

Inhibition of Epigenetic Modifiers LSD1 and HDAC1 Blocks Rod Photoreceptor Death in Mouse Models of Retinitis Pigmentosa

Evgenya Y. Popova,[1,2] Yuka Imamura Kawasawa,[3] Samuel Shao-Min Zhang,[1,2] and Colin J. Barnstable[1,2]

[1]Department of Neural and Behavioral Sciences, Penn State University College of Medicine, Hershey, Pennsylvania 17033, [2]Penn State Health Eye Center, Hershey, Pennsylvania 17033, and [3]Departments of Pharmacology and Biochemistry and Molecular Biology, Institute for Personalized Medicine, Penn State College of Medicine, Hershey, Pennsylvania 17033

Epigenetic modifiers are increasingly being investigated as potential therapeutics to modify and overcome disease phenotypes. Diseases of the nervous system present a particular problem as neurons are postmitotic and demonstrate relatively stable gene expression patterns and chromatin organization. We have explored the ability of epigenetic modifiers to prevent degeneration of rod photoreceptors in a mouse model of retinitis pigmentosa (RP), using rd10 mice of both sexes. The histone modification eraser enzymes lysine demethylase 1 (LSD1) and histone deacetylase 1 (HDAC1) are known to have dramatic effects on the development of rod photoreceptors. In the RP mouse model, inhibitors of these enzymes blocked rod degeneration, preserved vision, and affected the expression of multiple genes including maintenance of rod-specific transcripts and downregulation of those involved in inflammation, gliosis, and cell death. The neuroprotective activity of LSD1 inhibitors includes two pathways. First, through targeting histone modifications, they increase accessibility of chromatin and upregulate neuroprotective genes, such as from the Wnt pathway. We propose that this process is going in rod photoreceptors. Second, through nonhistone targets, they inhibit transcription of inflammatory genes and inflammation. This process is going in microglia, and lack of inflammation keeps rod photoreceptors alive.

Key words: **chromatin; epigenetic; LSD1; rd10; retina degeneration; rod photoreceptor**

Significance Statement

Retinal degenerations are a leading cause of vision loss. RP is genetically very heterogeneous, and the multiple pathways leading to cell death are one reason for the slow progress in identifying suitable treatments for patients. Here we demonstrate that inhibition of LSD1and HDAC1 in a mouse model of RP leads to preservation of rod photoreceptors and visual function, retaining of expression of rod-specific genes, and with decreased inflammation, cell death, and Müller cell gliosis. We propose that these epigenetic inhibitors cause more open and accessible chromatin, allowing expression of neuroprotective genes. A second mechanism that allows rod photoreceptor survival is suppression of inflammation by epigenetic inhibitors in microglia. Manipulation of epigenetic modifiers is a new strategy to fight neurodegeneration in RP.

Introduction

The epigenetic landscape of a cell defines the potential patterns of gene expression, including transcriptional responses to a changing environment. There are increasing efforts to modify the epigenome both to channel normal development and to combat a variety of diseases. Many of these studies have been conducted on dividing cells, particularly tumor cells. The nervous system presents a very different substrate for epigenetic modification because neurons are postmitotic.

The retina continues to be a valuable model for studies of the role of the epigenome in both normal and pathophysiological conditions. Dynamic regulation of photoreceptor gene expression in the retina is governed not only by an array of specific transcription factors (TFs) but also by changing patterns of epigenetic regulation through histone modifications and resulting changes in overall chromatin structure (Popova et al., 2012; Aldiri et al., 2017; Hughes et al., 2017; Norrie et al., 2019; Tan et al., 2019). Two major classes of histone modifications are methylation and acetylation of lysine residues in the histone tail

Received Dec. 10, 2020; revised June 11, 2021; accepted June 18, 2021.

Author contributions: E.Y.P., C.J.B., and S.S.-M.Z. designed research; E.Y.P. and Y.I.K. performed research; E.Y.P., C.J.B., and Y.I.K. analyzed data; E.Y.P. and C.J.B. wrote the paper.

This work was supported by grants to C.J.B. from the National Institutes of Health (EY029992) and the Pennsylvania Tobacco Settlement Fund. We thank Dr. Alistair Barber and Dr. Stephanie Grillo for help in the visual function assay on a CerebralMechanics OptoMotry system.

The authors declare no competing financial interest.

Correspondence should be addressed to Colin J. Barnstable at cbarnstable@psu.edu.

https://doi.org/10.1523/JNEUROSCI.3102-20.2021

(N-terminal nonhelical region). Methylation is controlled by two antagonist sets of enzymes, lysine methyltransferases and demethylases (KDMs), whereas acetylation is regulated by histone acetyltransferases and histone deacetylases (HDACs). lysine-specific demethylase 1 (LSD1) demethylates histone H3K4me2/1, and together with class I HDACs, works as subunits of repressive chromatin complexes such as Sin3, nucleosome remodeling, and histone deacetylation; corepressor for element-1-silencing transcription factor; and nuclear receptor corepressor/silencing mediator for retinoid or thyroid hormone receptors (Shi et al., 2005; Sun et al., 2010; Whyte et al., 2012). Inhibition of either LSD1 or HDAC1 enzymes during early postnatal mouse retina development leads to a suppression of rod photoreceptor differentiation (Popova et al., 2016; Ferreira et al., 2017).

Retinitis pigmentosa (RP) is an inherited form of retinal degeneration that is characterized by the death of rod photoreceptors followed by secondary loss of cone photoreceptors. RP is very heterogeneous with more than 4000 identified mutations in over 100 genes/loci (for updates of retinal disease genes, see https://sph.uth.edu/retnet/). This is one reason for the slow progress in identifying suitable treatments for patients. Several enzymes participating in the process of chromatin compaction and gene repression are upregulated in mouse models of RP (Sancho-Pelluz et al., 2010; Arango-Gonzalez et al., 2014; Farinelli et al., 2014).

Certain mouse mutations recapitulate many of the features of human retinitis pigmentosa. In the rd10 mouse line the rod-specific gene Pde6b is mutant, the same gene that is altered in one form of autosomal recessive retinitis pigmentosa in humans (McLaughlin et al., 1993; Chang et al., 2002, 2007; Hart et al., 2005; Won et al., 2011; Charish et al., 2020). In these animals the mutation reduces but does not eliminate PDE6 activity, and they display a phenotype where most retina cells reach terminal maturation before degeneration starts. Rapid degeneration happens between postnatal (P) day 17 and P25, with complete loss of rods observed by P45–60 (Chang et al., 2002, 2007; Gargini et al., 2007).

Here we demonstrate that inhibition of LSD1 or HDAC1 in rd10 mice leads to rod photoreceptor preservation and maintenance of visual function. Analysis of the array of gene expression changes induced by these inhibitors leads us to suggest that they suppress expression of key inflammatory genes and also induce more open and accessible chromatin, which in turn allows expression of genes from a variety of neuroprotective mechanisms. Manipulation of epigenetic modifiers represents a new strategy to fight neurodegeneration in RP.

Materials and Methods

Antibodies and reagents. Chemicals were purchased from Fisher Scientific, unless otherwise noted. The 0.9% bacteriostatic sodium chloride was from APP Pharmaceuticals. LSD1 inhibitors, trans-2-phenylcyclopropylamine [parnate or tranylcypromine (TCP)] was purchased from Tocris Bioscience, and GSK2879552 was from Selleckchem.com. The HDAC inhibitor romidepsin was from Sigma. Anti-rhodopsin (RHO) monoclonal antibodies have been described previously (Barnstable, 1980) and react with an N-terminal sequence shared by many species The commercial antibodies used were the following: anti-H3K4me2 (catalog #07-030, Millipore), anti-H3K9me2 (catalog #ab1220, Abcam), anti-GFAP (catalog #MAB360, Millipore), anti-IBA1 (for the *Aif1* gene; catalog #019-19741, FUJIFILM Wako Pure Chemical), anti-OPN1SW (catalog #AB5107, Millipore), anti-PRDE6B (catalog #PA1-722, Thermo Fisher Scientific), and anti-β-actin (ACTB; catalog #A4700, Sigma).

Animals. Wild-type C57Bl/6J (catalog #000664), and rd10 B6.CXB1-Pde6brd10/Jrd10 (catalog #004297) mice were purchased from The Jackson laboratory and housed in a room with an ambient temperature of 25°C, 30–70% humidity, a 12 h light–dark cycle, and *ad libitum* access to rodent chow. This study was conducted using both male and female mice in accordance with the National Research Council's Guide for the Care and Use of Laboratory Animals (eighth edition), and all animal experiments were approved by the Penn State University College of Medicine Institutional Animal Care and Use Committee (protocol #46 993).

Treatment with LSD1 and HDAC1 inhibitors. Mice were treated daily with intraperitoneal injections (i.p.) of trans-2-phenylcyclopropylamine (parnate or TCP) at 10 mg/kg, GSK2879552 at either 1.5 mg/kg or 4.2 mg/kg, romidepsin at 0.2 mg/kg, or saline as control. All inhibitors were diluted in 0.9% bacteriostatic sodium chloride (saline).

Tissue collection. Whole retinas were isolated from animals by removing the sclera and most of the retinal pigmented epithelium layer under PBS. Right-eye retinas from each animal were taken for RNA extraction, cDNA preparation, and reverse transcription-polymerase chain reaction (RT-PCR). Immediately after isolation, tissue was flash frozen in liquid nitrogen and stored at −80°C. Left eye retinas from each animal were subjected to fixation, cryopreservation, sectioning, and immunofluorescence staining.

RNA extraction and cDNA preparation. RNA extraction and purification followed the manufacturer's protocol from RNeasy Mini Kit and RNA shredder (Qiagen). Final RNA concentrations were determined spectrophotometrically using a NanoDrop 1000 Spectrophotometer (Thermo Fisher Scientific). cDNA was synthesized with SuperScript II, III, or IV First-Strand Synthesis System kit according to the manufacturer's protocol (Invitrogen).

RT-PCR. Primers were purchased from Integrated DNA Technologies (IDT). The sequence information is listed in Table 1. For quantitative real-time PCR we used 2 × iQ SYBR Green PCR supermix from Bio-Rad Laboratories. Samples in triplicate were run on an iQ5 Multicolor Real Time PCR Detection System (Bio-Rad). The relative expression level for each gene was calculated by the 2-ΔΔCt method and normalized to GAPDH. Genes were considered upregulated or downregulated if $p < 0.05$.

RNA-sequencing. RNA was extracted from P24 retina of wild-type (WT) and rd10 animals treated with saline or GSK from P9 until P24. RNA integrity number (RIN) was measured using Bioanalyzer (Agilent) and RNA 6000 Nano Kit (Agilent) to confirm RIN above seven for each sample. The cDNA libraries were prepared using the Illumina Stranded mRNA Prep Ligation kit according to the manufacturer's instructions. Briefly, poly A RNA was purified from 200 ng of total RNA using Oligo (dT) beads. The extracted mRNA fraction was subjected to fragmentation, reverse transcription, end repair, 3′–end adenylation, and adaptor ligation, followed by PCR amplification and solid phase reversible immobilization bead purification (Beckman Coulter). The unique dual index sequences (IDT for Illumina RNA UD Indexes Set A, Ligation) were incorporated in the adaptors for multiplexed high-throughput sequencing. The final product was assessed for its size distribution and concentration using Bionalyzer High Sensitivity DNA Kit (Agilent). The libraries were pooled and diluted to 3 nM using 10 mM Tris-HCl, pH 8.5, and then denatured using the Illumina protocol. The denatured libraries were loaded onto an S1 flow cell on an Illumina NovaSeq 6000 and run for 2 × 53 cycles according to the manufacturer's instructions. Demultiplexed and adapter-trimmed sequencing reads were generated using Illumina bcl2fastq (released version 2.20.0) allowing no mismatches in the index read. BBDuk was used to trim/filter low-quality sequences using the qtrim=lr trimq = 10 maq = 10 option. Next, alignment of the filtered reads to the mouse reference genome (mouse Ensembl release 67 (GRCm37/NCBIM37/mm9) was done using HISAT2 (version 2.1.0) applying the –no-mixed and –no-discordant options. Read counts were calculated using HTSeq by supplementing Ensembl gene annotation (release 67: "Mus_musculus.Ensembl.NCBIM37.67.gtf"). The edgeR package was used to fit the read counts to the negative binomial model along with the generalized linear model, and differentially expressed genes were determined by the likelihood

Table 1. Primer sequences to study gene expression

Gene	Forward primer	Reverse primer
Aifm1	TGCTCTTGGCAGAAAGTCTC	TGGGCATCACTTTCACTCC
Apaf1	GTACACCCCCTGAAAAGCAA	CAGGGTGGGTCACCATCTAT
Bcl2	AGCCCGTGTTTGTAATGGAG	CACAGCCTTGATTTTGCTGA
Bdnf	GAGCGTGTGTGACAGTATTAGCG	CATGGGATTACACTTGGTCTCG
C1qa	GAGGGGAGCCAQGAGCTG	GGATTGCCTTTCACGCCC
C1qb	GCTGATGAAGACACAGTGGG	GCTGTTGATGGTCCTCAGG
Capn2	CCCCAGTTCATTATTGGAGG	GCCAGGATTTCCTCATTCAA
Casp9	CAG GCC CGT GGA CAT TGG TT	CAG CCG CTC CCG TTG AAG ATA
Ccnd1	Qiagen #QT00154595	
Cd74	CAAACCTGTGAGCCAGATGC	GGTCCTGGGTCATGTTGC
Cnga1	AATACGTGGCATTCCTTCGTAAA	GAGCCATTGTCATCGTCAGAAA
Cngb1	AGAGGAGGAACACTACTGCG	AAGTAATCCATGAGGAGCCAGA
Crx	Qiagen QT00115402	
Cst7	CGAACTACATGCAGGAAGACC	CACTGGCAGAGGAGAACAGG
Cx3cr1	CAGCATCGACCGGTACCTT	GCTGCACTGTCCGGTTGTT
Foxn4	GTG AGA TCT ACA GCT TCA TGA AGG	TGA GAT GAG CTT GTC CAA CTC C
Foxp1	GGTTGTACAGCAGTTAGAGCTACAG	GGAGTATGAGGTAAGCTCTGTGG
Gapdh	Qiagen QT01658692	
Gfap	GAGAGAAAGGTTGAATCGCTGG	CGGCGATAGTCGTTAGCTTC
Gnat2	ACCATGCCTCCTGAGTTG	TGACTCTGGATCGAAGCAC
H2-Aa	GTCTTGACTAAGAGGTCAAATTCC	TTCTGAGCCATGTGATGTTG
Hes1	TTC CAA GCT AGA GAA GGC AGA C	GCA CCT CGG TGT TAA CGC
Hes5	AAGCTGCTGCTGGAGCAG	GCAGCTTCATCTGCGTGTC
Neurod1	CCT GTG ACC TTT CCC ATG C	AGA AGT GCT AAG GCA ACG C
Nr2e3	CTTCAAACCTGAAACACGAGG	CCTCAAAGATGGGAGCAGGAG
Nrl	GTGCCTCCTTCACCCACCTTCAGTGA	GCGTGCGGCGCCTCTGCTTCAGCCG
Opn1sw	CAGCATCCGCTTCAACTCCAA	GCAGATGAGGGAAAGAGGAATGA
Otx2	TCG CCA CCT CTA CTT TGA TAG	AGC CGC ATT GGA CGT TAG
Pde6b	CTG ACG AGT ATG AGG CCA AAG	TAG GCA GAG TCC GTA TGC AGT
Pde6c	CCT TAT GTG GTC AGC CAA TAA AG	CCA TCT GGA GTC TTT GGT CC
Prph2	TGGATCAGCAATCGCTACCT	CTGTAGTAATTCAGCAGAGC
Ptp4a3	TACAGAGCTTCCTCCAAGGAAA	CACGGTGTTGGGAACGG
Ptprc	TGCCTCACCTACACACACC	ACATGAGTCATTAGACACACTGATG
Rgr	TTG TGT GGA TGT CAT CTG C	GAA GTG TGT GTG ATG AAC AGG
Rho	CTT CTC CAA CGT CAC AGG CGT	GGACCACAGGGCGATTTCAC
Rlbp1	AGCAGGGCTTTGATGGTAGC	TTCAGCTCATCCTTGGCCTTC
Rom1	Qiagen #QT00172165	
Rorb	CCGTCAGAATGTGTGAGAACCAG	ATCCTCCCGAACTTTACAGCATC
Sag	GCC ATG AGT GTC CTC ACC	GGC ATG CTG CAC TTT CC
Samd11	CTT TCT GGC TGT GGC GAG	GCC ATG TAG AAG ACA CGG C
Smad3	GTGAAGAAGCTCAAGAAGAC	ACTGGAGGTAGAACTGGCGTC
Sox2	GAGTGGAAACTTTTGTCCGAG	GAAGCGTGTACTTATCCTTCTTCAT
Tfap2b	Qiagen #QT00135478	
Thrb	GTTTTCCCTCTCGTCCATCAGAGGACCTG	GCTTCCGCTTGGCTAGCCTCTTGCT
Vsx2	ACGGAGCTCCCAGAAGAC	CCATCCTTGGCAGACTTG

ratio test method implemented in edgeR. Significance was defined to be those with a q value <0.05, calculated by the Benjamini–Hochberg method to control the false discovery rate (FDR), and log2-fold change is >1 or smaller than -1. The ggplot2 R package was used for generating heatmaps. Raw counts and differential expression analysis generated during this study are available at Gene Expression Omnibus, submission GSE169527.

Pathway, Gene Ontology, and upstream regulator analysis. Ingenuity Pathways Analysis (IPA) was used to identify upstream regulators and significantly enriched canonical pathways with the following cutoff of FDR <0.05 and fold change in gene expression >2 or $<1/2$. The Database for Annotation, Visualization, and Integrated Discovery (DAVID) was used for Gene Ontology (GO) functional analysis.

Immunofluorescence staining. Retinas were fixed in 4% paraformaldehyde overnight at 4°C, washed in PBS, incubated in 5% sucrose/PBS for 30 min, and then cryopreserved in 20% sucrose/PBS overnight at 4°C. Retinas were embedded in a 2:1 mix of 20% sucrose and optimum cutting temperature (OCT; Sakura Finetek) and stored at −80°C. Blocks with tissue samples were sectioned to 7–10μm on a Cryostat Microtome HM550 (Thermo Fisher Scientific) and stored at −20°C. Antigen retrieval was performed by incubating the slides in 10 mM sodium citrate, pH 6, for 30 min at 80°C. Double labeling immunohistochemistry was performed as previously described (Popova et al., 2016; Ferreira et al., 2017) using fluorescent Alexa Fluor conjugated secondary antibodies diluted 1:800 (Invitrogen). Primary antibodies were diluted as follows: anti-H3K4me2, 1:600; anti-H3K9me2, 1:600; anti-RHO, 1:50; anti-OPN1SW, 1:400; anti-GFAP, 1:1000; and anti-IBA1, 1:450 (*Aif1* gene). Slides were counterstained with Hoescht 33258 (1 mg/ml diluted 1:1000) and visualized using an Olympus Fluoview FV1000 confocal microscope. The acquisition parameters were maintained constant for each set of experiments. Fluorescence intensity was assessed using ImageJ software.

Western blot. Both retinas from one animal were flash frozen together in liquid nitrogen and stored at −80°C. Samples for SDS-PAGE were prepared by resuspended retinas in 50 μl PBS. Laemmli sample buffer was added, samples were boiled for 10 min, resolved on Criterion TGX Precast Gel AnyKD (Bio-Rad), transferred to nitrocellulose membrane, and immunoblotted with antibodies anti-H3K9me2 or anti-H3K4me2 diluted 1:5000, anti-ACTB diluted 1:10,000, and anti-PDE6B diluted 1:500. Secondary goat anti-rabbit/mouse HRP (Jackson ImmunoResearch) was diluted 1:5000. An ECL Western Blot Detection system (Thermo Fisher Scientific) was used to visualize the bound of the primary antibody.

Chromatin immunoprecipitation. Lysate preparation for chromatin immunoprecipitation (ChIP) was conducted as before (Popova et al., 2016; Ferreira et al., 2017). In brief, 10 mouse retinas were rapidly isolated and rinsed in PBS on ice. Cell suspensions in PBS were cross-linked with 1% formaldehyde for 15 min at room temperature, followed by quenching with 1 M glycine, incubation on ice for 5 min, and centrifugation for 7 min at 4000 rpm at 4°C. Pellets were resuspended in 500 μl L-CHIP buffer (1% SDS, 10 mM EDTA, 50 mM Tris-HCl, pH 8.0), 1 mM PMSF and 10 μl protease inhibitor mix (Sigma), sonicated twice at setting 3 for 10 s on Sonic Dismembrator (Fisher Scientific, Model 100). Protein concentrations were adjusted to 1 mg/ml with L-CHIP buffer. ChIP was performed as described in (Popova et al., 2012) and subjected to quantitative PCR. Primers for genomic regions are specified in Table 2.

Visual function. A CerebralMechanics OptoMotry system was used to evaluate visual function in control and GSK each second day (ESD) in rd10 mice. Spatial frequency (SF) threshold and contrast sensitivity (CS) were assessed using a video camera to monitor optomotor reflex. CS was assessed at an SF of 0.092 cycles/degree. SF was assessed at 100% contrast. The CS and SF thresholds were identified as the highest values that elicited the reflexive head movement. SF (acuity) was measured on P24, P26, P28, and P32 and then averaged; during this time acuity in GSK-treated animals slowly increased, whereas control mice acuity was diminished. CS was measured three times on P33–35, when control mice were blind.

TUNEL assay. Retinas were fixed in 4% paraformaldehyde overnight at 4°C, washed in PBS, incubated in 5% sucrose/PBS for 30 min, and then cryopreserved in 20% sucrose/PBS overnight at 4°C. Retinas were embedded in a 2:1 mix of 20% sucrose and OCT (Sakura Finetek) and stored at −80°C. Blocks with tissue samples were sectioned to 7–10μm on a Cryostat Microtome HM550 (Thermo Fisher Scientific) and stored at −20°C. TUNEL assay was conducted using the In Situ Cell Death Detection Kit, Fluorescein (Roche) according to the manufacturer's instruction. Sections were counterstained with Hoescht 33258 (1 mg/ml diluted 1:1000), washed three times with PBS, and analyzed by confocal microscopy.

Statistical analyses. Results are presented as means ± SEM. Unpaired one-tail Student's t test (two tailed, unpaired) was used to evaluate statistical significance between groups; p value <0.05 was considered significant. Statistical analyses for experiments were performed using GraphPad Prism software.

Results

LSD1 and HDAC1 inhibitors preserve rod photoreceptors in mouse models of retinitis pigmentosa

We have previously shown that LSD1 and HDAC1 inhibitors have dramatic effects on the expression of rod photoreceptor

Table 2. Primer sequences to assay ChIP

Gene name	Forward primer	Reverse primer	Target region
Bdnf	AGCTGCGGGTATCTCCATAA	AGGCTGAGATCCTAGGCAGA	Promoter
Ccnd1	TTA GAA TAA AGC GGT TCC ACC	TTCGGAGCTACAGTGGAATC	Promoter
Crx	GCTCAGGTTGGCCTCAGAC	CCACACTAGTGCGAGACCTGAG	Promoter
Foxn4	GGACTTTGATCCTGCTGCAAG	CAAGGGTTCTAGGAAATGGTCC	Intragenic, H3K4me2 max in embrio
Foxp1	AGATAGAAGGTGCAGCAAGAAGG	AGTTGTAACTCCAAACCTTGCG	Promoter
Gnat2	GAACAGAGACTGCAGAGACAGATC	AATCTTGATGGTGTCTGATATTGG	Intragenic, CRX, NRL binding
Hes1	GCC TGG CCA CAA AAG AAA TA	CCCAAACTTTCTTTGCCACA	Proximal promoter
Otx2	CACGGTCACTTCTCCACAGCG	CCCCATTCCCCTTTGCACTG	Promoter
Pde6b	CAGGACCCGTTTCATCAG	GGTGTTCCTGCTGCTGTG	Promoter
Rgr	CAGGCAAGCTACAGACCTCAG	TAATATGCAGGAATCCTTCATGG	Enhancer in the end of gene
Rho	GGAATTCCCAGAGGACTCTG	CTCTTCGTAGACAGAGACC	Promoter
Smad3	TGAAGCCCACACAGGAAGTG	CTATAAGCATCCATATGCACTGTGG	Intragenic
Sox2	AAAGCACTCTAGTAAAAGCAAGTCC	GGTGTACTATTACGCTCAACACG	Enhancer end of loop
Vsx2	TTCTGCTGCTGTTCCTCATTTAC	CTAATAACGATGGTATTGGCTCAG	Proximal promoter

genes during retinal development (Popova et al., 2016; Ferreira et al., 2017). We have now tested a mouse model of retinitis pigmentosa to determine whether the changes induced by these inhibitors could also offset the degenerative changes found in this disease. The phenotype of rd10 is illustrated in Fig. 1*A*, where loss of rods is apparent by P19, most photoreceptors have disappeared by P24, and photoreceptor loss is complete by P60.

We treated rd10 mice daily with i.p. of the HDAC1 inhibitor romidepsin, the LSD1 inhibitors TCP and GSK2879552, or control saline for 15 d beginning at P9, several days before degeneration is detectable, and ending at P24, when most rod photoreceptors have normally been lost.

In control rd10 mice injected with saline only, two to three rows of photoreceptors remained in the outer nuclear layer (ONL) of the retina. Based on antibody staining most of these were rods, although the lengths of their outer segments (OS) were diminished (Fig. 1B). Treatment of rd10 mice with romidepsin at a concentration of 2 mg/kg (suggested for mice; Bishton et al., 2011; Jain et al., 2015) was harmful as mice were dying during such treatment. Lower concentrations of romidepsin also increased mortality, but we were able to use a concentration of 0.2 mg/kg, and we could see the effect of the treatment, although mice were not healthy (discussed later). Under romidepsin inhibition an average of eight rows of photoreceptor remained in the ONL at P24, but OS were not so pronounced as after TCP treatment (Fig. 1*B*,*D*). Treatment with TCP at a concentration of 10 mg/kg (Kerenyi et al., 2013; Shi et al., 2013) partly protected ONL with on average seven rows of photoreceptors remaining at P24 (Fig. 1*B*,*D*) with longer OS. The best retina ONL preservation was achieved when we treated rd10 mice with the more specific LSD1 inhibitor GSK (Mohammad et al., 2015). We started with the concentration suggested for mice, 1.5 mg/kg, but the effect on photoreceptor preservation was mild (five to six rows of photoreceptors remain; data not shown), so we increased the dose to 4.2 mg/kg, and all subsequent experiments were performed with this concentration. Treatment with this concentration of GSK led to preservation of >10 rows of photoreceptors (Fig. 1*B*,*D*), almost to the level of WT retina ONL (Fig. 1*D*,*E*) with normal length OS. RHO protein staining was also increased under GSK inhibition (Fig. 1*C*). In addition to counting photoreceptor rows in ONL, we measured the overall ONL thickness (Fig. 1*E*). The patterns of changes in ONL thickness closely followed the changes in the number of photoreceptors rows in ONL.

Continuous presence of LSD1 inhibitors is needed to prevent rod degeneration in a retinitis pigmentosa model

We next conducted a series of experiments to investigate the time course of the effects of GSK treatment. First, we examined the result of beginning the injection of GSK at a later time point. Treating mice with GSK from P15 to P24 blocked further degeneration (Fig. 2*A*,*E*, pink bars). Treatment from P9 to P17 showed minimal degeneration when the retinas were examined at P17 but substantial loss of photoreceptors at P24, 1 week after ending treatment (Fig. 2*B*,*E*, gray bars). Similarly, when mice were treated with our original time course, from P9 to P24, the preservation of rod photoreceptors seen at P24 decreases over the next 21 d so that at P45, there had been a substantial loss of cells (Fig. 2*C*,*E*, yellow bars). These results argue that GSK can block but not reverse degeneration and that its continued presence is necessary to prevent further rod photoreceptor degeneration in the rd10 mutant.

We also tested whether daily doses of GSK were necessary. We treated mice ESD with GSK 4.2 mg/kg for the same length of time as before, and in these conditions photoreceptors have survived to essentially the same extent as with treatment each day (Fig. 2*D*,*E*, green bars).

During all treatments we monitored the weight gain of animals. All mice treated with inhibitors, both mutant and WT, showed less weight gain when compared with saline-injected controls (Fig. 3*A*,*B*). The smallest increase in body weight was observed with romidepsin treatment. GSK in a smaller concentration of 1.5 mg/kg or injecting a higher 4.2 mg/kg ESD did not show any significant difference in body weight gain from controls.

Treatment of rd10 mice with an LSD1 inhibitor increases visual function

As ESD-treated mice had better movement and reflexes, we tested visual functions in this group of mice using optometry reflex (Prusky et al., 2004). After treatment with GSK, rd10 mice demonstrated much better acuity than saline-treated controls (Fig. 2*F*), where untreated mutant animals have spatial frequency threshold around only 0.085cyc/deg, whereas GSK-injected mice have a threshold ~0.240cyc/deg. Acuity in WT mice reached a maximum of 0.4 cyc/deg, so our treatment preserves ~60% of vision in rd10 mice. Spatial frequency was measured on P24, P25, P26, P28, and P32, and during this time frame acuity in GSK-treated animals slowly increased, whereas in untreated mice acuity was

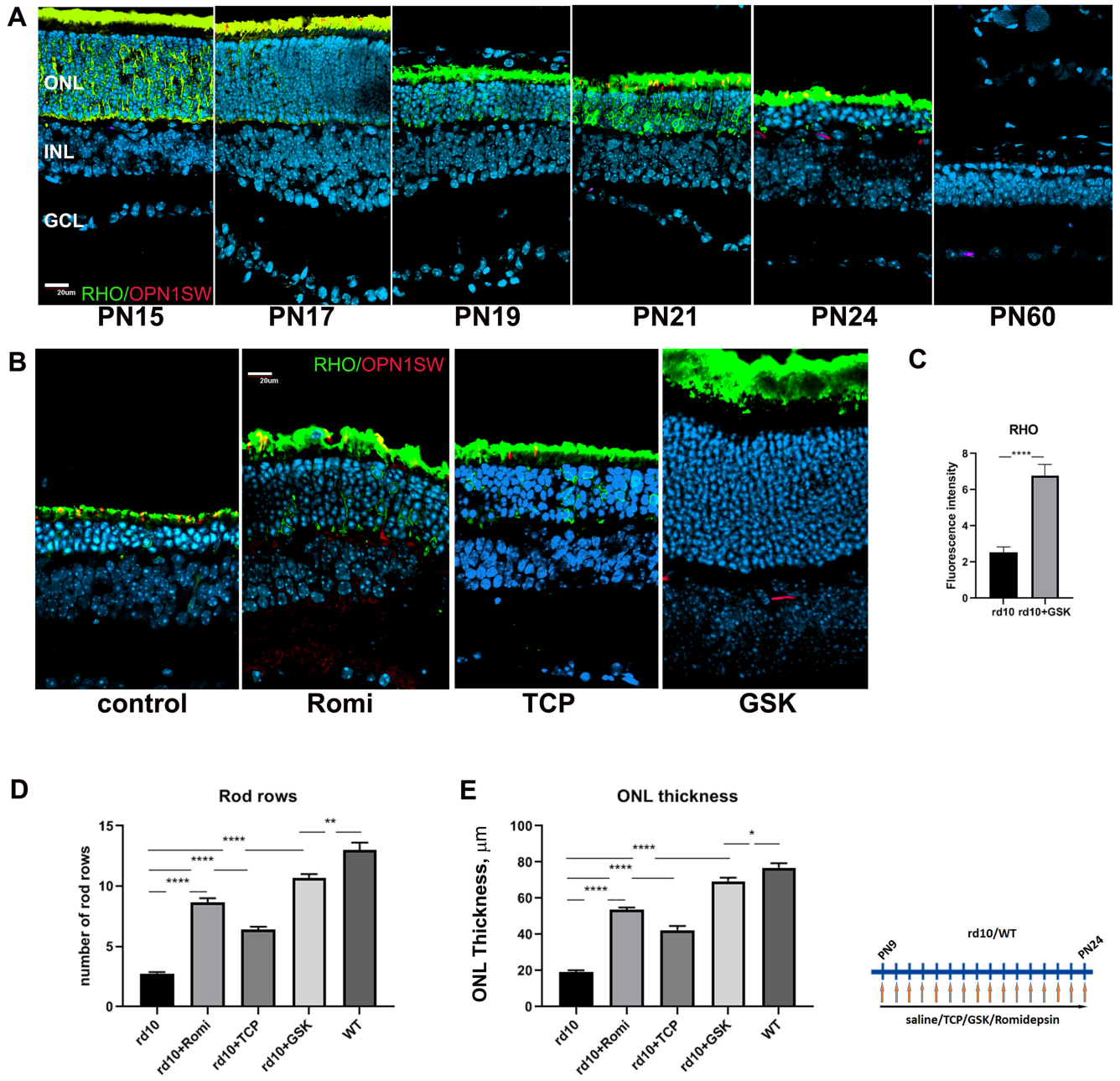

Figure 1. Treatment of rd10 mice with inhibitors specific for LSD1 and HDAC1 leads to neuroprotection and preservation of rod photoreceptors. ***A***, Immunofluorescence microscopic images of sections of retinas from rd10 mice from P15 to P60 stained with RHO (green), OPN1SW (red), and nuclear counterstained with Hoechst33358 (blue); GCL, Ganglion cell layer. Scale bar, 20 μm. ***B***, Immunofluorescence microscopic images of retina sections from P24 rd10 mice treated from P9 until P24 with inhibitors for HDAC1 (romidepsin) or LSD1 (TCP and GSK) or only saline (control), stained with RHO (green), OPN1SW (red), and nuclear counterstained with Hoechst33358. ***C***, Image quantification of immunofluorescence intensity for RHO was conducted for four biological and three technical replicates (±SEM) for the rd10 retinas treated with GSK or saline (control); $^{****}p < 0.0001$. ***D***, Rods rows were counted in central retina for P24 mice treated from P9 until P24 with inhibitors for LSD1 (TCP and GSK) and HDAC1 (romidepsin) or only with saline (WT and rd10) for three to five biological and three technical replicas (±SEM); $^{**}p < 0.01$, $^{****}p < 0.0001$. ***E***, ONL thickness was measured in the central retina for P24 mice treated from P9 until P24 with inhibitors for HDAC1 (romidepsin), LSD1 (TCP and GSK), or only with saline (WT and rd10) for three to five biological and three technical replicates (±SEM) for each sample; $^{*}p < 0.05$, $^{**}p < 0.01$, $^{***}p < 0.001$, $^{****}p < 0.0001$.

diminished (data not shown). Additionally, GSK-treated mice had contrast sensitivity 43.4 ± 14.6% at 0.092 c/d spatial frequency when measured at P33–35. Maximum contrast sensitivity in WT mice reached 95% at this spatial frequency, so our treatment preserved ~50%. At this age the control rd10 mice were blind. Thus, inhibition of LSD1 in mouse models of RP not only leads to morphologic rod photoreceptor preservation, but also helps to maintain visual function.

Inhibitor specific for LSD1 alters retinal gene expression in rd10 mice

After establishing that treatment of mouse models of retinitis pigmentosa with inhibitors specific for LSD1 and HDAC1 led to morphologic and functional preservation of rod photoreceptors, we next studied how this treatment influences gene expression. We performed RNA sequencing (RNA-seq) on retina samples from rd10 and WT mice treated with GSK inhibitor or saline from P9 until P24 (Fig. 4). Using a cutoff of FRD <0.05 and a

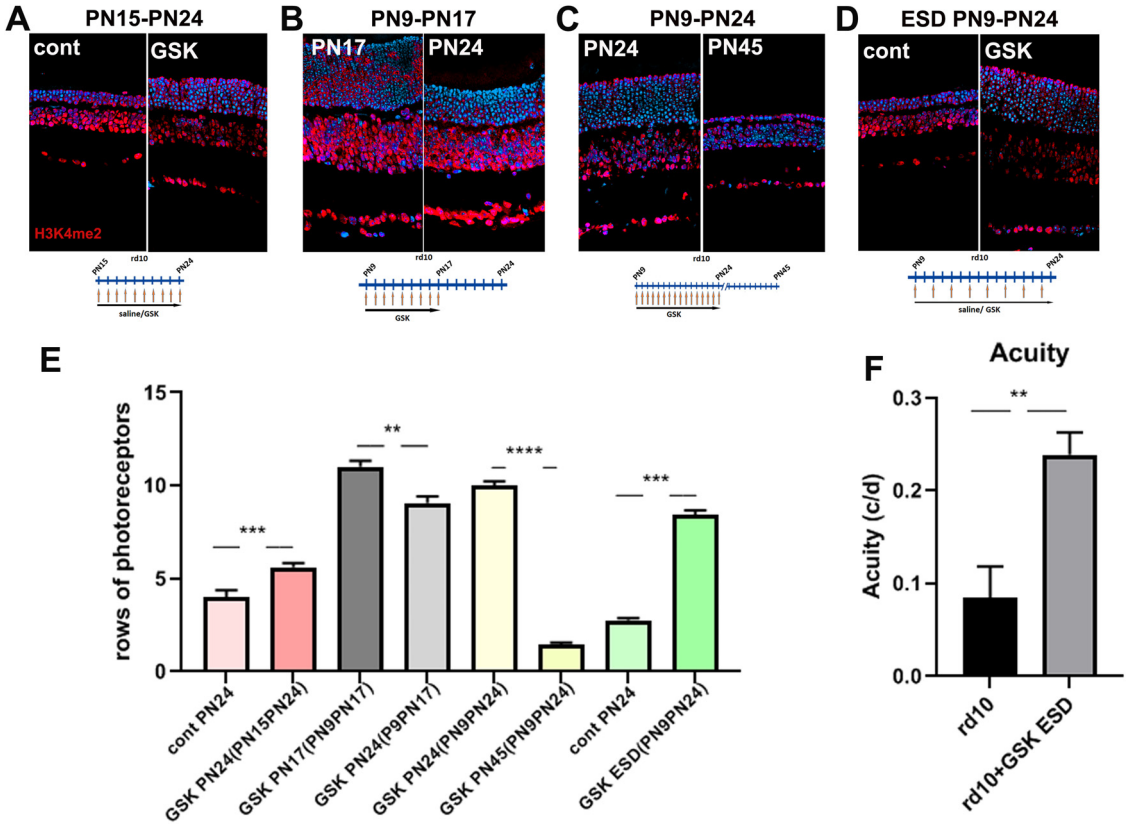

Figure 2. Continuous presence of LSD1 inhibitors is needed to prevent rod degeneration in a retinitis pigmentosa model. ***A–D***, Immunofluorescence microscopic images of sections of rd10 mouse retinas treated with LSD1 inhibitor GSK at different time frames, stained with anti-H3K4me2 antibody (red) and nuclear counterstained with Hoechst33358 (blue). Treatment with GSK from P15 until P24, assayed at P24 and compared with controls treated with saline only (***A***). rd10 mice litter was treated with GSK from P9 until P17; half litter assayed at P24, half assayed at P17, and compared P24 to P17 (***B***). rd10 mice litter was treated with GSK from P9 until P24: half litter assayed at P24, half assayed at P45, and compared P45 to P24 (***C***). rd10 mice were treated with saline or with GSK each second d (ESD) from P9 until P24 (***D***). ***E***, Rods rows were counted in central retina for rd10 mice for three to five biological and three technical replicas (±SEM); $^{**}p < 0.01$, $^{***}p < 0.001$, $^{****}p < 0.0001$. Time frames correspond to ***A*** (pink/red bars), ***B*** (gray bars), ***C*** (yellow bars), ***D*** (green bars). ***F***, Evaluation of visual function in rd10 mice treated from P9 until P32 with saline (control) and GSK ESD. Spatial frequency (SF) threshold were assessed using a video camera to monitor optomotor reflex. SF was assessed at 100% contrast. The SF thresholds were identified as the highest values that elicited the reflexive head movement. SF (acuity) was measured for six eyes of rd10 control and six eyes for rd10 treated with GSK ESD on P24, P25, P26, P28, and P32 and then averaged for each eye; $^{**}p < 0.01$.

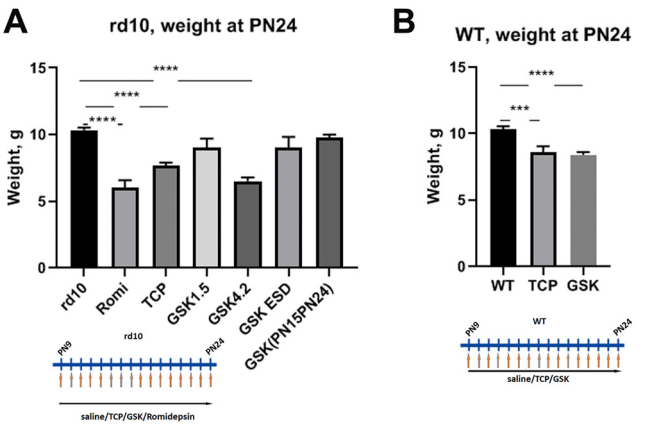

Figure 3. Treatment of mice with inhibitors specific for LSD1 and HDAC1 slow gain of weight. ***A***, Weight of mice at P24 after rd10 mice were treated from P9 until P24 with romidepsin, TCP, GSK 1.5, GSK 4.2 mg/kg, and GSK 4.2 ESD. ***B***, WT mice were treated with saline, GSK, or TCP. Experiments were done for three to five biological replicas; $^{***}p < 0.001$, $^{****}p < 0.0001$ (±SEM).

fold change (FC) >2 or <0.5, rd10 mice treated with GSK had 719 genes upregulated and 369 genes downregulated, whereas WT mice treated with GSK only upregulated 77 genes and downregulated 13 genes (Fig. 4*A*).

With more relaxed criteria ($p < 0.05$ and a fold change >1.75 or <0.8) we found ~150 genes that were simultaneously upregulated in rd10 and WT mice retina under GSK inhibition (Fig. 4*B*). We hypothesized that these differentially expressed genes (DEG) found in both rd10 and WT are upregulated because of global effects on chromatin structure and accessibility. To test this we examined the chromatin state, using our (Popova et al., 2012) and others' databases (Aldiri et al., 2017) for adult WT mice retina. Of the 147 genes that have annotation in the RefSeq database, 39 DEG are in heterochromatin, 8 are on the border between euchromatin and heterochromatin, and 8 are in euchromatin but show decreasing expression during development. Fifty-three DEG have no histone epigenetic marks, H3K27 or H3K4me2, and 57 DEG have more inhibitory marks (H3K27me3), than active marks (H3K4me2). These findings demonstrate that the majority of the DEG simultaneously upregulated by GSK in rd10 and WT mice belong to normally repressed or silent chromatin compartments in adult retina, and their upregulation under LSD1 inhibition indicates an opening of chromatin. The H3K4me2 histone modification is a marker not only of transcribed genes but also of enhancers, and 38 DEG genes that were in euchromatin are in a vicinity of developmental superenhancers (+/50 kb). Among upregulated common genes were developmental transcriptional factors (*Cited4*, *Foxf1*, *Gsc2*, *Irf6*, *Lefty2*, *Mesp1*, *Mesp2*, *Myod1*, *Pax7*, *Sox10*, *Zcchc12*) and genes participating in eye development and homeostasis (*Arhgap36*,

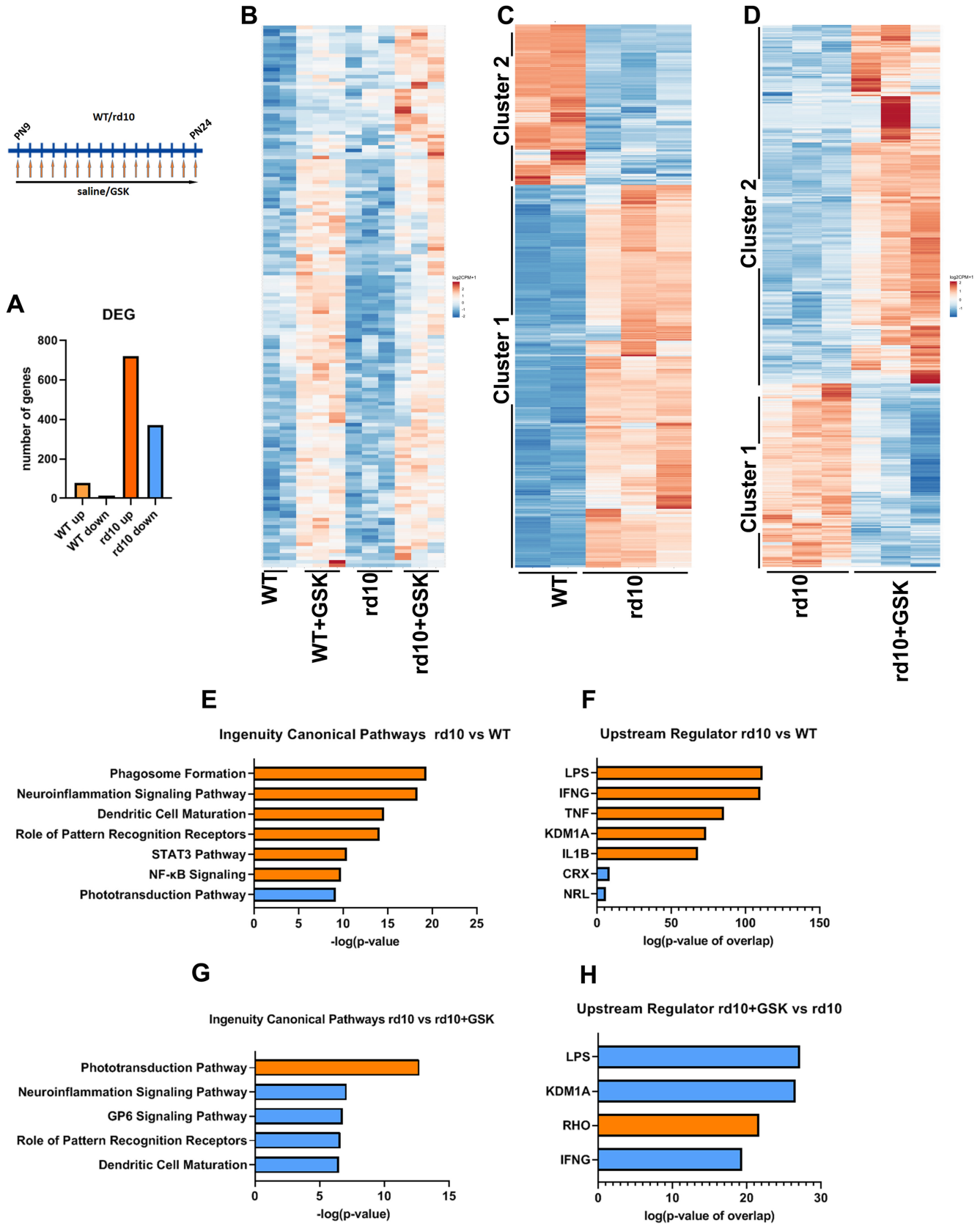

Figure 4. RNA-seq analysis of altered retinal gene expression under LSD1 inhibition. ***A***, Overall changes in number of genes up and down regulated in WT and rd10 mice treated by GSK and compared with saline-treated controls (FDR < 0.05; FC > 2 or < 0.5). RNA-seq was done for two WT, three WT+GSK, three rd10, and three rd10+GSK retinal samples. ***B***, Heatmap of DEG simultaneously upregulated in rd10 and WT mice retinas under GSK treatment [$p < 0.05$; FC >1.75 or <0.8). ***C***, Heatmap of DEG between WT and rd10 retinas (FDR <0.05; FC >2 or <0.5). ***D***, Heatmap of DEG between rd10 and treated with GSK rd10 retinas (FDR <0.05; FC >2 or <0.5). ***E***, Top, Ingenuity canonical pathways for DEG between WT and rd10 retinas (FDR <0.05; FC >2 or <0.5) according to IPA. ***F***, Top, Upstream regulators according to IPA for DEG between WT and rd10 retinas (FDR <0.05; FC >2 or <0.5). ***G***, Top, Ingenuity canonical

Table 3. Functional enrichment for gene clusters in Figure 4*C* identified using a Web-based DAVID classification tool and GO categories

Cluster	WT versus rd10	Biological process	Cellular component	Molecular function
Cluster 1	UP in rd10	Immune system process	Extracellular region	Integrin binding
		Innate immune response	Cell surface	Heparin binding
		apoptotic process	Phagocytic vesicle membrane	Peptide antigen binding
		Phagocytosis	External side of plasma membrane	TNF-activated receptor activity
		Positive regulation of inflammatory response	Pernuclear region of cytoplasm	2′–5′-oligoadenylate synthetase activity
Cluster 2	DOWN in rd10	Visual perception	Photoreceptor outer segment	Structural constituent of eye
		Response to stimulus	Photoreceptor inner segment	Intracellular cGMP-activated cation channel activity
		Phototransduction	Cell projection	Haptoglobin binding
		Cilium assembly	Extracellular matrix	Transporter activity
		Neurotrasmitter transport		

Table 4. Functional enrichment for gene clusters in Fig.4*D* identified using a Web-based DAVID classification tool and GO categories

Cluster	rd10 vs rd10+GSK	Biological process	Cellular component	Molecular function
Cluster 1	DOWN in rd10+GSK	Immune system process	Membrane	Peptide antigen binding
		Innate immune response	External side of membrane	2′–5′-oligoadenylate synthetase activity
		Pyroptosis, cytolysis	Extracellular exosome	Beta-2-microglobulin binding
		Phagocytosis engulfment	Cell surface	Cytokine receptor activity
		Interleukin-1 beta production	NLPR1 inflammasome complex	Carbohydrate binding
Cluster 2	UP in rd10+GSK	Visual perception	Photoreceptor outer segment	Structural constituent of eye
		Response to stimulus	Extracellular matrix	Bicarbonate transmembrane transport activity
		Positive regulation of rhodopsin gene expression	Photoreceptor inner segment	Protein heterodimerization activity
		Phototransduction	Extracellular region	cGMP binding
		Retinol metabolic process	Z disk	

Baiap3, *Ccno*, *Cutal*, *Crabp2*, *Gng8*, *Lrat*, *Mapk15*, *Sfrp5*, *Sypl2*). Several genes belong to the Wnt pathway and could play an important role in neuroprotection (*Fam83g*, *Lefty2*, *Sfrp5*, *Upk1b*).

We next analyzed genes and pathways that were differentially expressed in rd10 in comparison to WT retinas (Fig. 4*C*). Two clusters readily classified the DEG. In cluster 1, genes were upregulated in rd10, and in cluster 2, genes were downregulated in rd10. IPA demonstrated that pathways associated mostly with inflammation and phagocytosis were activated (cluster 1), whereas the phototransduction pathway was inhibited (cluster 2; Fig. 4*E*). Upstream regulators for activated pathways, according to IPA, were LPS, IFNG (interferon), TNF, IL6B—all connected to inflammation—and upstream regulators for inhibited pathways were CRX (conerod homeobox gene) and NRL (neural retina leucine; Fig. 4*F*).

We then identified DEG in rd10 retina under LSD1 inhibitor (Fig. 4*D*). Again, all genes sorted into two clusters, where cluster 1 comprises genes that are downregulated in rd10+GSK retinas, and cluster 2 consists of genes that are upregulated in rd10+GSK. IPA indicated that the major upregulated pathway is the phototransduction pathway (Fig. 4*G*). The next four most important downregulated pathways were all related to neuroiflammation (Fig. 4*G*). According to IPA, top upstream regulators were LPS and IFNG, connected to inflammation pathways, and RHO (rhodopsin), connected to the phototransduction pathway (Fig. 4*H*). The key finding was that KDM1a (another name for LSD1) is the second most important upstream regulator. This supports the recent finding that LSD1 can act on nonhistone targets to regulate the inflammatory response (Kim et al., 2018; Oh et al., 2020).

We extended our study of the RNA-seq data with a GO analysis of the functions of DEG in rd10 compared with WT retina (Table 3) and in rd10+GSK compared with rd10 (Table 4). The top biological processes that were upregulated in rd10 and reverted by GSK treatment are innate immune response and immune system process; the most crucial cellular components were membrane, external side of plasma membrane, and extracellular region. Molecular functions were 2′−5′ oligoadenylatase activity, peptide antigen binding, and cytokine receptor activity. The most essential biological processes that were downregulated in rd10 and reverted by GSK were visual perception, response to stimulus, and phototransduction; the top cellular components were photoreceptor outer and inner segments and extracellular matrix. The top molecular functions were structural constituents of eye and cGMP binding.

We next explored what type of immune cells participated in the inflammation process in rd10 retinas and what type of immune cells were the major targets for GSK inhibition. Known cell markers for Müller glia, such as *Rlbp1, Slc1a3*, *Glast*, *Ptbp1*, *Cralbp1*, and *Glul* were not changed in rd10 versus WT or in rd10 versus rd10+GSK according to RNA-seq data. However, some Müller cell markers of damaged retinas (Kang et al., 2020), including *Lcn2*, *Serpina3e*, *Gfap*, *Cxcl10*, *Timp1*, and *Ccl2* were upregulated in rd10 in comparison with WT, but not all of them returned to a WT level of expression in rd10+GSK retinas. On the other hand, many more markers for activated microglia and infiltrating immune cells were upregulated in rd10 retinas (markers; Ronning et al., 2019). Expression of resident microglia markers *Atp6v0d2*, *Mcoln3*, *Cd5l*, *Ctsd*, *C1qa*, *Fcrls*, *Hexb*, *Gpr34*, *Junb*, *Pclaf*, and *Birc5* were upregulated in rd10 and went back to normal levels of expression in rd10+GSK. Expression of markers of infiltrating immune cells, such as monocytes and macrophages *H2-Aa*, *cd74*, *H2-Ab1*, *H2-Eb1*, *Cyp4f18*, *Ms4a6c*, *Lyz2*, *Ms4a7*, *4930430Erik*, *Apoe*, *Hp*, *Ly6c2*, and *Cx3cr1* were also upregulated

←

pathways for DEG between rd10 and treated with GSK rd10 retinas (FDR <0.05; FC >2 or <0.5) according to IPA. ***H***, Top, Upstream regulators according to IPA for DEG between rd10 and treated with GSK rd10 retinas (FDR <0.05; FC >2 or <0.5). In all panels orange color represents upregulated gene or activated pathway; blue color represents downregulated gene or inhibited pathway. FC = fold change; DEG = differentially expressed genes; FDR = false discovery rate.

in rd10 and returned to normal levels of expression in rd10+GSK. This suggests that the major inflammatory mediators in rd10 were associated with microglia and that these were susceptible to inhibition by LSD1 inhibitors.

Validation of RNA-seq results by qPCR

We next confirmed selected results of the RNA-seq experiments using qRT-PCR, where genes were considered upregulated or downregulated if the expression was significantly different from untreated control rd10 animals with a p value <0.05. Allowing for the different thresholds and sensitivities of the methods, our qPCR results verify the conclusions of the RNA-seq study. Each of the classes of genes validated by qPCR are described and illustrated in the following sections.

Changes in rod photoreceptor gene expression

First, we analyzed the changes in rod-photoreceptor-specific genes (Fig. 5*A*) including the following: (1) genes expressed early in development, such as *Rom1*and *Neurod1*; (2) genes expressed in mature rods, such as *Rho* and *Sag*; and (3) transcription factors, such as *Crx* and *Nrl*. The treatment of rd10 mice with LSD1 inhibitors TCP or GSK increased expression of almost all rod genes in retina relative to GAPDH, confirming the RNA-seq results. In comparison, there were no changes in rod photoreceptor genes expression in retina in WT mice treated with TCP (data not shown) or GSK (Fig. 5*A*).

With GSK treatment, expression of one group of rod-specific genes, *Rho*, *Prph2*, *Nr2e3*, *Nrl*, and *Pde6b*, was increased dramatically and reached WT level (Fig. 5*B*, top row). Expression of other rod-specific genes, *Sag*, *Rom1*, *Crx*, *Cnga1*, and *Cngb1* was increased but not to the WT level (Fig. 5*B*, bottom row).

We also analyzed the effects of treatment with the HDAC1 inhibitor romidepsin in rd10 mice. This compound had the strongest effect on early rod genes but very little effect on most late rod genes or TFs (Fig. 5*A*).

Although the expression of the Pde6b gene was maintained under LSD1 and HDAC1 inhibition (Fig. 5*A*; RNA-seq data), this measurement was of RNA and not protein. We used Western blots to demonstrate a three-fold increase of Pde6b protein in retinas treated with inhibitor GSK (Fig. 5*C*).

Additionally, we examined how expression of rod-specific genes changed when studied at alternative time windows of i.p. injection with epigenetic modulators (Fig. 6, compare with Fig. 2). The changes in expression of markers were closely correlated with the preservation of OS and rods in ONL after treatment for rd10 (Fig. 6); for example, for *Rho* levels the correlation coefficient is $r^2 = 0.92$ between the number of rod rows in retinas and *Rho* expression (data not shown). Thus, the changes in rod photoreceptor genes expression are probably a reflection of the number of rods preserved in the treated rd10 mice.

Changes in cone photoreceptor gene expression

From the RNA-seq data, although expression of genes specific for rod photoreceptors were returned to normal expression levels in rd10+GSK retina, most genes specific for cone photoreceptors, including *Opn1sw, Opn1mw*, *Thrb, Jam3*, *Pde6c*, *Pde6h*, *Otop3*, and *Gnat2* did not show changes that met the threshold criteria in either rd10 versus WT or in rd10 versus rd10+GSK. We studied this in more detail using RT-PCR. Treatment of rd10 mice with epigenetic inhibitors had small but detectable effects on expression of cone genes (Fig. 7*A*). In general, expression of cone markers was slightly lower in rd10 at P24 than in WT retinas, and treatment with GSK did not change it (Fig. 7*B*). Some cone genes were slightly upregulated (*Thrb* or *Gnat2*) in rd10 treated with TCP or GSK but downregulated following romidepsin treatment (Fig. 7*A*). We additionally estimated changes in cone-specific genes under ESD treatment and showed that except for S-opsin, expression of all other cone genes was increased to WT levels (Fig. 7*C*), thus demonstrating that proper GSK treatment not only had a neuroprotective effect on rod photoreceptors but also helped preserve cones.

Changes in gene expression of other retina cell types

RNA-seq data demonstrated that markers for other retina cell types did not show changes that met the threshold criteria in either rd10 versus WT or in rd10 versus rd10+GSK, except two markers of amacrine cells *Clrn1* and *Efemp1* that were upregulated in rd10 and downregulated under GSK inhibition. According to qRT-PCR, expression of most other retina cell type markers examined appeared to be decreased especially under GSK and romidepsin inhibition, with the exception of *Rgr* and *Hes5* genes (Fig. 7*A*). GSK treatment of rd10 mice caused an increase in *Rgr* and *Hes5* expression (Figs. 7*A*, 8), corroborating the RNA-seq data. This suggests that LSD1 inhibition has specific effects on the expression of these genes.

Decreased expression of gene markers of nonphotoreceptor retinal cell types could be either because epigenetic inhibitors are harmful for INL cells or is a result of preserving the number of photoreceptors and decreasing percentage of others cell types in rd10 retinas. To distinguish between these two possibilities, we treated rd10 retinas with GSK at later stages from P30 until P40, when retinas in rd10 mice consist mostly of INL cell types (Fig. 8). Gene expression did not change, suggesting that epigenetic inhibitors are not harmful for retina cells in the INL, but the increase in proportion of photoreceptors in the retina leads to an apparent decrease in relative expression of specific genes from other retina cell types.

LSD1 and HDAC1 inhibitors decrease cell death, gliosis and inflammation

We first compared the amount of cell death in control rd10 and rd10 treated with TCP by TUNEL staining. In both cases only a very small number of dying cells was detected with no significant difference between them (Fig. 9*B*). Different mechanisms of rod photoreceptors deaths have been suggested in the literature (Iribarne and Masai, 2018; Wang et al., 2018; Power et al., 2020a, b), so we assayed several genes that provide us with a broader understanding of processes occurring in the retina during treatment with epigenetic inhibitors GSK and romidepsin. Expression of apoptotic-specific genes BclII, *Apaf1*, and *Casp9* was slightly decreased (Fig. 9*A*; Tiwari et al., 2015). Similarly, expression of the calcium-activated protease calpain 2 (*Capn2*), and its substrate apoptosis-inducing factor (*Aifm*1), was somewhat decreased in rd10 mutant mice treated with epigenetic inhibitors (Fig. 9*A*). The RNA-seq data identified only a small number of genes participating in different pathways of cell death that were upregulated in rd10, including *Capn9*, *Casp1*, *4*, *8*, *12*, *Aif1* (IBA1 protein), *Ripk3*, and *Mlkl*; some of these were downregulated under GSK inhibition [*Capn9*, *Casp1*, *12*, *Aif1* (IBA1 protein)].

GFAP is a marker of both Müller glia and astrocytes, and increased levels of GFAP expression is characteristic of gliosis, a glial response to any damage in the nervous system. According to the RNA-seq data, *Gfap* was increased in rd10 and then decreased under GSK inhibition, but this decrease did not reach our threshold conditions. We found that both gene expression of

A

	Gene	WT+GSK	RD10+TCP	RD10+GSK4.2	RD10+Romi		
Rod late	Rho		*	**		fold change	
	Pde6b		**	****	**	>3	down
	Prph2		**	****	*	2-3	
	Sag		***	****		1.75-2	
Rod early	Rom1		*	****	****	1.5-1.75	
	Ptp4a3			****	***	1.2-1.5	
	Neurod1			****	****	0.83-1.2	
	Samd11	*	*	****	**	1.2-1.5	
Photoreceptor TF	Nrl		**	****		1.5-1.75	
	Rorb		***	****		1.75-2	
	Nr2e3		***	**	**	2-3	
	Crx		***	**		>3	up
	w/o * - not significant						

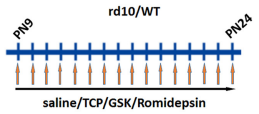

B

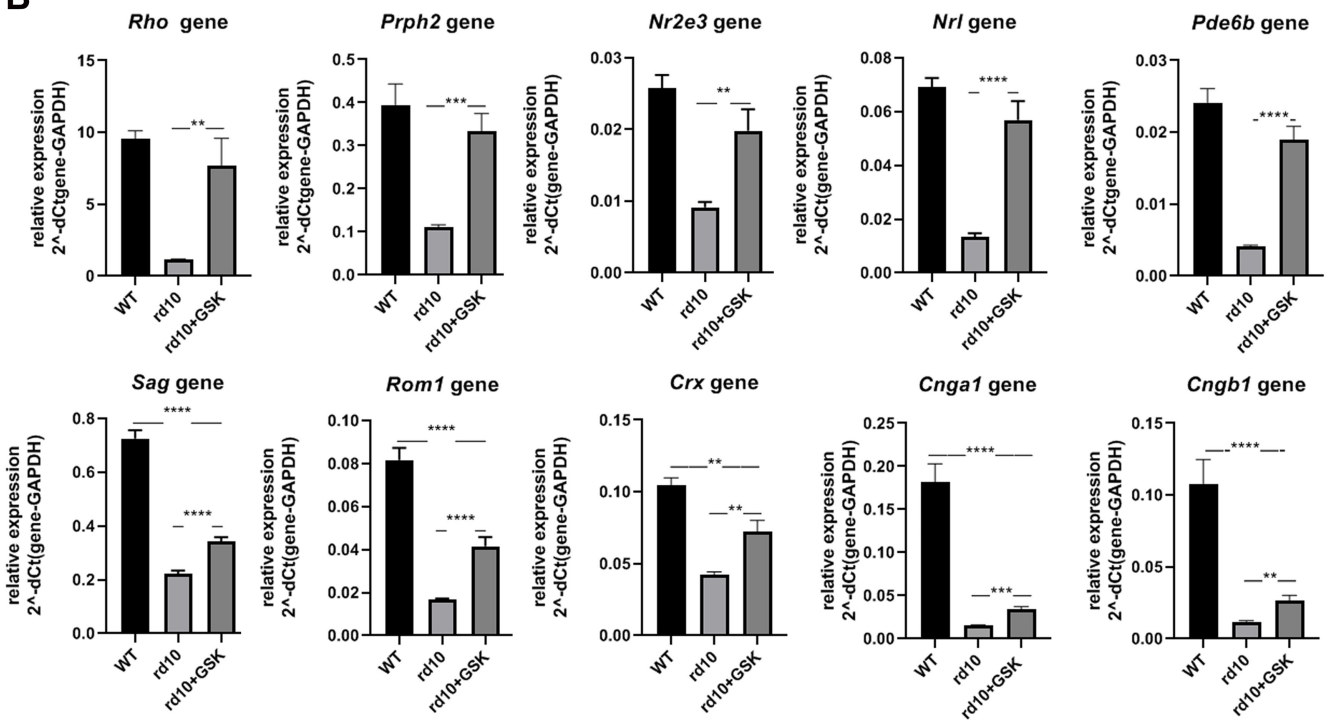

C

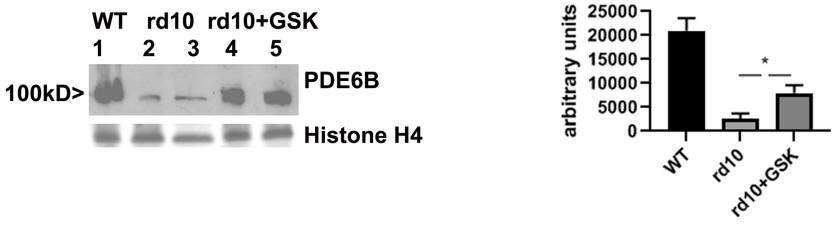

Figure 5. Treatment of mouse model of retinitis pigmentosa with inhibitors specific for LSD1 and HDAC1 leads to preservation of expression of rod-specific genes. ***A***, Heatmap of expression of different groups of rod-specific genes measured by RT-PCR for retinas from P24 rd10 (or WT) mice treated from P9 until P24 with inhibitors for LSD1 (TCP and GSK) and HDAC1 (romidepsin) compared with controls rd10 (or WT) mice treated with saline only for three to five biological and three technical replicas (±SEM). The relative expression level for each gene was calculated by the 2-ΔΔCt method and normalized to GAPDH. *$p < 0.05$, **$p < 0.01$, ***$p < 0.001$, ****$p < 0.0001$ with fold increase in orange or decrease in green. ***B***, Comparison of rod-specific gene expression levels in mice P24 retina of WT mice and rd10 mice treated with saline or in rd10 treated with GSK from P9 until P24. Experiments were done for four biological and three technical replicas. ** $p < 0.01$, ***$p < 0.001$, ****$p < 0.0001$. ***C***, Increasing of PDE6B protein level. Anti-PDE6B Western blot with representative samples of retina at P24 from WT mice treated with saline and rd10 mice treated with saline or with GSK from P9 until P24. Histone H4 Coomassie staining was used as loading control. Band intensity quantification was done using three to five biological and three technical replicates for anti-PDE6B Western. For each sample, anti-PDE6B bands intensity was normalized to the average of quantified intensities of Coomassie bands for histone H4 and anti-ACTB Western band.

		A	B	C	D	E		
	comparison	GSK saline	TCP saline	GSK saline	PN24 GSK PN17 GSK	PN45 GSK PN24 GSK		
	injections time	PN9 to PN24 ESD	PN10 to PN29	PN15 to PN24	PN9 to PN17	PN9 to PN24		fold change
	assay time	PN24	PN40	PN24	PN24	PN45	down	>3
Cell Type Specificity	Gene							2-3
Rod late	Rho	***	**			****		1.75-2
	Prph2	****	nd			****		1.5-1.75
	Sag	****	*		***	****		1.2-1.5
Rod early	Rom1	***	*			****		0.83-1.2
Photoreceptor TF	Nrl	****	*			****		1.2-1.5
	Rorb	**	nd		***	****		1.5-1.75
	Crx	****			****	****		1.75-2
Cone	Gnat2	****			**			2-3
Photoreceptor rows		****	****	***	**	****	up	>3
		w/o * - not significant						

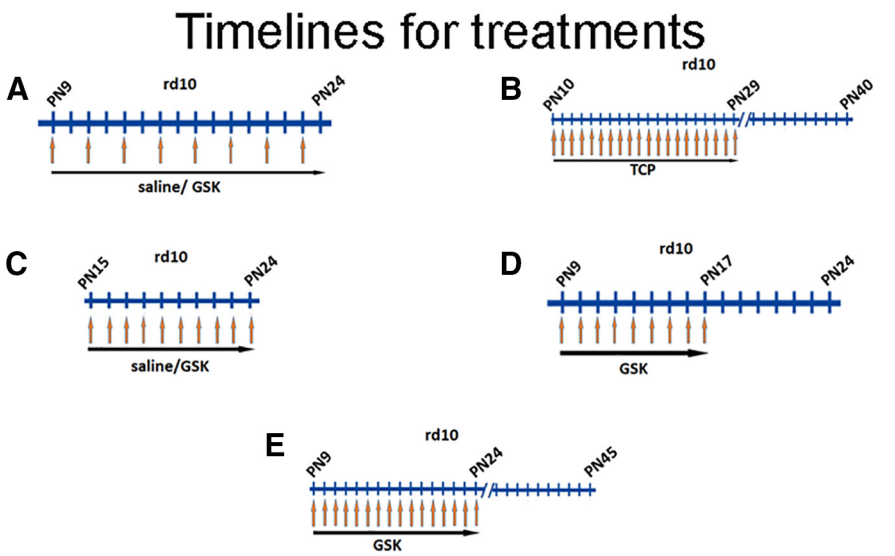

Figure 6. Changes in expression of retina gene markers are close correlates with rod preservation if alternative time windows were used for i.p. injection of epigenetic inhibitors. Heatmap of expression of different groups of genes measured by RT-PCR and rod rows counted in central retina for retinas from mice treated with inhibitors for LSD1 (TCP and GSK) for three to five biological and three technical replicas (±SEM). $^{**}p < 0.01$, $^{****}p < 0.0001$. The relative expression level for each gene was calculated by the 2-ΔΔCt method and normalized to GAPDH. $^{*}p < 0.05$, $^{**}p < 0.01$, $^{***}p < 0.001$, $^{****}p < 0.0001$ with fold increase in orange or decrease in green. Column A, rd10 mice were treated with GSK from P9 until P24 each second d, assayed at P24, and compared with controls treated with saline only. Column B, rd10 mice were treated with TCP from P10 until P29, assayed at P40, and compared with controls treated with saline only. Column C, rd10 mice were treated with GSK from P15 until P24, assayed at P24, and compared with controls treated with saline only. Column D, rd10 mice litter was treated with GSK from P9 until P17; half litter assayed at P24, half assayed at P17, and compared P24 to P17. Column E, rd10 mice litter was treated with GSK from P9 until P24: half litter assayed at P24, half assayed at P45, and compared P45 to P24.

Gfap (Figs. 7*A*, 9*D*), and immunofluorescence labeling of the GFAP protein (Fig. 9*C*,*E*) demonstrated upregulation in rd10 retinas relative to WT and reductions in Müller cell activation of GSK-treated retinas. We obtained similar results with TCP treatment (data not shown). We also labeled retina sections for IBA1 (*Aif1* gene), a marker for microglia. IBA1 labeling was significantly increased in multiple layers of rd10 compared with WT, and although the labeling was decreased by GSK/TCP treatment, the levels remained above WT (Fig. 9*C*; data not shown). This mirrors the increase and decrease in Aif1 RNA that was detected by RNA-seq (see above) and qRT-PCR (Fig. 9*G*). We conclude that in rd10 both Müller cells and microglia show responses and that treatment with inhibitors leads to a decrease in gliosis in Müller cells.

Because inhibition of HDAC1 with romidepsin also preserved retinas from degeneration in rd10 mice (Figs. 1, 5*A*), we examined whether it exerted the same effects on inflammatory genes as LSD1 inhibition. Following romidepsin treatment, the expression level of *Gfap* did not changed (Fig. 7*A*). Similarly, immunofluorescence labeling for GFAP and IBA1 (*Aif1* gene) did not demonstrate significant differences between rd10 and rd10+romidepsin retinas (Fig. 9*C*; data not shown). Expression levels for inflammatory markers were downregulated under HDAC1 inhibition, including the pan-leucocytes marker *Ptprc* (Cd45), pan-microglia marker *C1qa,* activated microglia marker *C1gb*, a marker of activated resident microglia *Cst7*, markers of infiltrating macrophages *H2-Aa* and *Cd74,* chemokine receptor *Cx3cr1*, and *Aif1* (IBA1 protein; Fig. 9*F*). RNA levels of H2-Aa, C1qa, *Aif1*, and Cxc3cr1 were also all reduced by treatment with GSK (Fig. 9*G*). We concluded from this that romidepsin treatment inhibited microglia activation on the level of RNA in the same way as GSK but was less powerful at the protein level for proteins such as GFAP and IBA1.

LSD1 inhibition promotes epigenetic changes that create more open and accessible chromatin in rod nuclei and make rods less mature

The range of gene expression changes and the changes in epigenetic marks that we noted earlier suggested that epigenetic

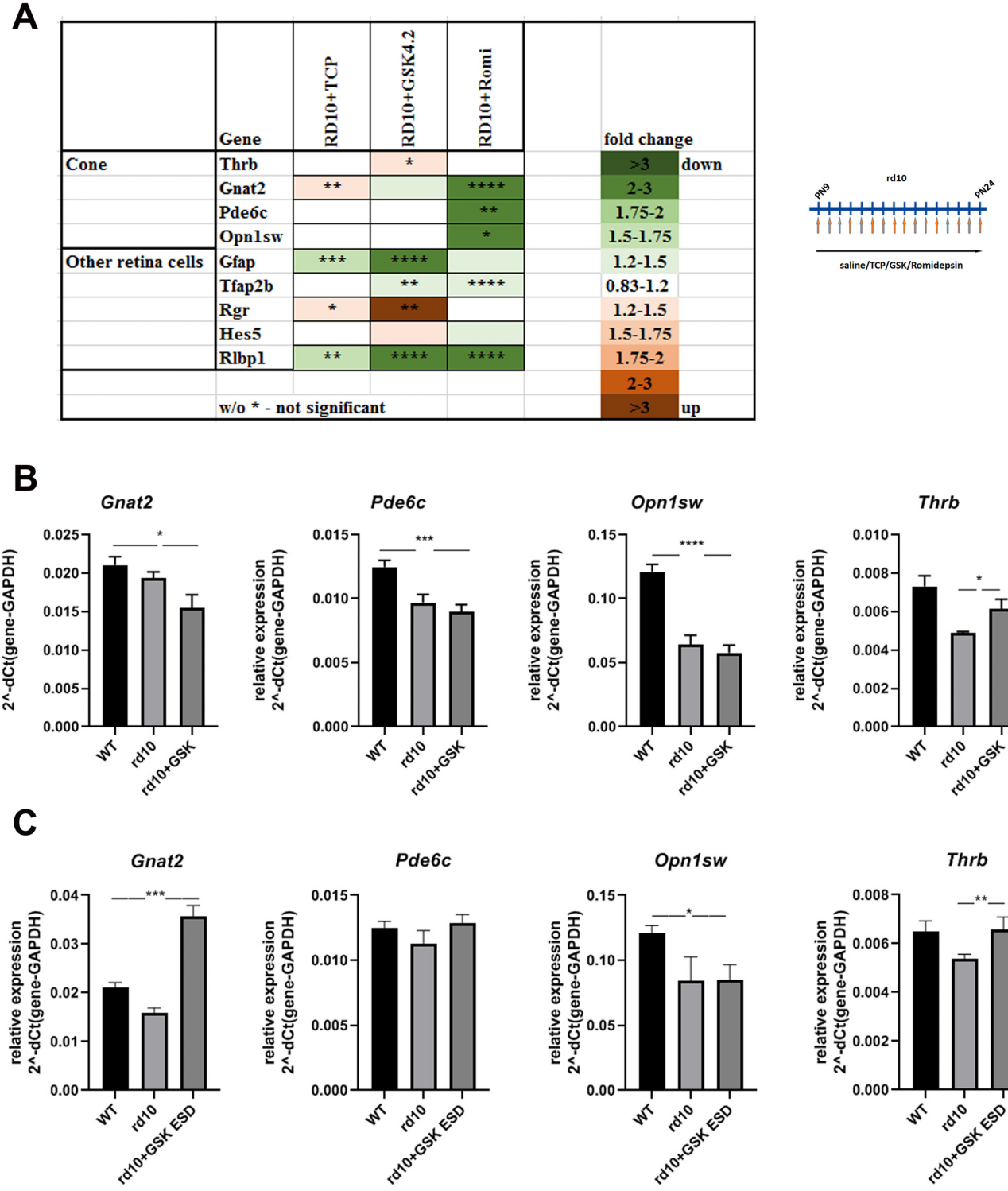

Figure 7. Effect of treatment of mouse model of Retinitis Pigmentosa with inhibitors of LSD1 and HDAC1 on other retina cell types. ***A***, Heatmap of expression of different groups of retina genes measured by RT-PCR for retinas from P24 mice treated from P9 until P24 with inhibitors for LSD1 (TCP and GSK) and HDAC1 (romidepsin), compared with control rd10 mice treated with saline only for three to five biological and three technical replicates (±SEM). The relative expression level for each gene was calculated by the 2-ΔΔCt method and normalized to GAPDH. * $p < 0.05$, ** $p < 0.01$, *** $p < 0.001$, **** $p <$ 0.0001 with fold increase in orange or decrease in green. ***B***, Comparison of cone photoreceptor-specific gene expression levels in P24 retina of WT mice, rd10 mice treated with saline, or rd10 treated with GSK from P9 until P24. Data shown for four biological and three technical replicates. * $p < 0.05$, *** $p < 0.001$, **** $p <$ 0.0001. ***C***, Comparison of expression levels for cone genes in mouse retina at P24; WT mice were treated with saline, and rd10 mice were treated with saline or with GSK ESD from P9 until P24. Experiments were done for three to four biological and three technical replicates. * $p < 0.05$, ** $p < 0.01$, *** $p < 0.001$ (±SEM).

inhibitor treatments was having effects on chromatin structure. We noted that the number of rows of rods in WT did not change, but the ONL thickness was significantly increased (Fig. 10*A*) after treating WT mice with TCP as a control, suggesting less compact nuclei and cell bodies. During retina postnatal maturation, mouse rod photoreceptor nuclei undergo a dramatic transformation when foci or chromocenters of heterochromatin, which at P1 were seen located mostly at the nuclear periphery,

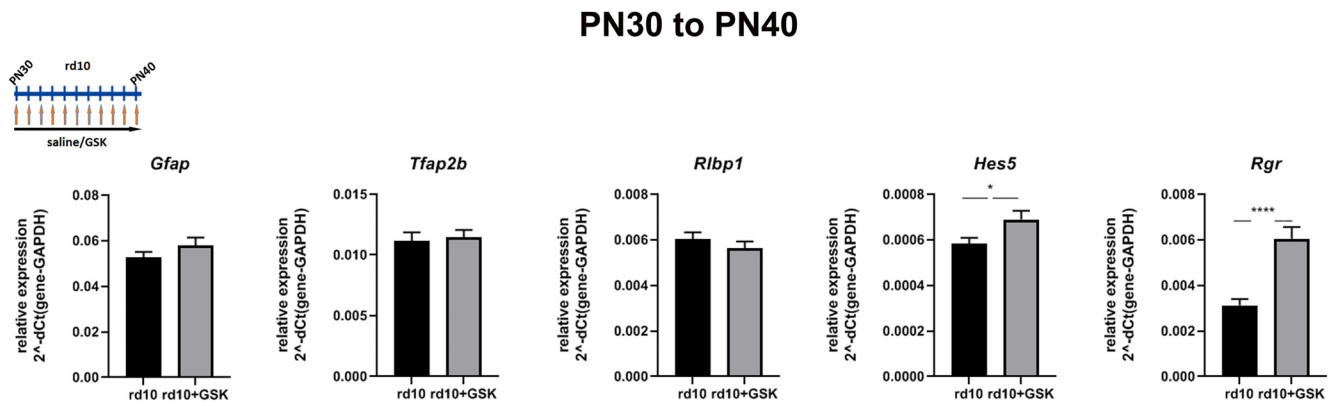

Figure 8. GSK treatment is not harmful for cells in INL. Comparison of gene expression levels in rd10 mice P40, retina treated with saline (control) or with GSK from P30 until P40. Experiments were done for five biological and three technical replicates. *$p < 0.05$, ****$p < 0.0001$ (±SEM).

around P15 began to relocate toward the center of the rod nuclei and started to fuse together so that at P28, rod nuclei have mostly two foci, and in adult eyes (P56) one big focus of heterochromatin occupied most of the nuclear volume pushing euchromatin out to the nuclear periphery (Solovei et al., 2009; Popova et al., 2013). We calculated the number of heterochromatin foci in rod nuclei to estimate the level of rod photoreceptor maturation in retinas of animals treated with LSD1 inhibitors (Fig. 10*B*). In WT animal retinas at P24, 55% rod nuclei have one focus, 43% have two foci, and only 2% have three foci; whereas in WT animals treated with TCP, fewer (42%) rod nuclei have one focus, 51% have two foci, and 7% have nuclei with three foci. In untreated rd10 animals the proportion of nuclei with one focus in the remaining rod photoreceptors is even bigger than in WT at 72%, and only 26% had two foci and 3% had three foci nuclei. Thirty-five percent of rod photoreceptor nuclei in rd10 retinas treated with GSK have one focus, 45% have two, and 20% have three foci (Fig. 10*B*). This demonstrates that treatment with LSD1 inhibitors leads to slower rod photoreceptor maturation and less compact heterochromatin in rod nuclei.

The enzymatic activities of LSD1 and HDAC1 remove active epigenetic methylation and acetylation marks, and inhibition of these enzymes should leave these active epigenetic marks intact (Riggs et al., 1977; Candido et al., 1978; Adamo et al., 2011; Kerenyi et al., 2013). To test whether the inhibitors could change epigenetic profiles of retinas, we used WT mice treated with TCP or GSK, but not rd10 mice, because rd10 retinas undergoing degeneration will have changes in cell type composition that will influence the epigenetic profile dramatically. Global levels of H3K4me2 did not change significantly following treatment with inhibitors as judged by Western blots (Fig. 10*C*). Additionally, we checked marks of facultative heterochromatin H3K9me2, which has been suggested as a substrate for LSD1 (Laurent et al., 2015). We did not see changes in global levels of H3K9me2 in retinas of treated mice (Fig. 10*C*).

Several TFs that participate in retina development and maturation showed a slightly increased expression in WT retinas treated with TCP or GSK (Fig. 10*D*). We used ChIP to measure whether there were changes in H3K4me2 marks on gene promoters or regulatory elements under GSK inhibition in WT mice for these genes. GSK-mediated LSD1 inhibition caused an increase in the methylation of H3K4 at the promoters/regulatory elements of most of these genes, for example, of cell cycle and progenitor genes *Ccnd1*, *Sox2*, and *Hes1*, as well as of rod-specific genes *Rho* and *Pde6b* (Fig. 10*E*, top). Although the overall level of H3K9me2 as detected on Western blots (Fig. 10*C*) did not change, probably because much of the H3K9me2 signal comes from mouse major satellite repeats, chromatin immunoprecipitation demonstrated that the regulatory elements of progenitor TF and rod-specific genes were losing this inhibitory mark (Fig. 10*E*, bottom) in retinas under GSK inhibition. This suggests that neuroprotective treatment with these epigenetic inhibitors leads to less mature and/or less compact but more open and accessible chromatin.

Discussion

Retinitis pigmentosa is a very heterogeneous disease with numerous different mutations and pathways leading to retina degeneration, suggesting that the most fruitful way to fight this disease needs to be gene independent. A number of molecular pathways have been implicated in triggering cell deaths of rod photoreceptors in RP (Newton and Megaw, 2020; Power et al., 2020b). These include dysregulation of cGMP- and Ca^{2+} signaling (Iribarne and Masai, 2018; Power et al., 2020a), insufficient proteasomal activity and accumulation of mis-folded proteins (Lobanova et al., 2018), oxidative stress (Trachsel-Moncho et al., 2018), and inflammation (Yoshida et al., 2013; Murakami et al., 2020).

We have demonstrated that inhibitors of two histone modification erasers, LSD1 and HDAC1, in a mouse model of RP (rd10), led to rod photoreceptor preservation (Fig. 1*B*,*D*,*E*) and retained expression of rod-specific genes (Figs. 4, 5) and maintenance of visual function (Fig. 2*F*). We also tested the effect of inhibiting LSD1 on degeneration in mice with more rapid retina degeneration, the rd1 mutant, but it was difficult to find an effective time frame for injection of epigenetic inhibitors because of the rapid deterioration of the retina before photoreceptors have fully developed. We identified two molecular mechanisms that account for this neuroprotective effect of the epigenetic inhibitors. First, acting on histone targets in photoreceptors, they increased accessibility of chromatin and upregulated neuroprotective genes (Figs. 4*B*, 10). Second, acting on nonhistone targets of LSD1 and HDAC1 in microglia, resident and infiltrating immune cells, they inhibit transcription of inflammatory genes and inflammation (Figs. 4*C*–*H*, 9>*C*–*G*; Tables 3, 4). Both mechanisms result in enhanced survival of functional rod photoreceptors.

Inhibition of the enzymatic activity of LSD1 and HDAC1 toward histone targets caused retention of active epigenetic marks in the genome of rod photoreceptors (Fig. 10*E*), epigenetic changes in heterochromatin organization of rod nuclei (Fig.

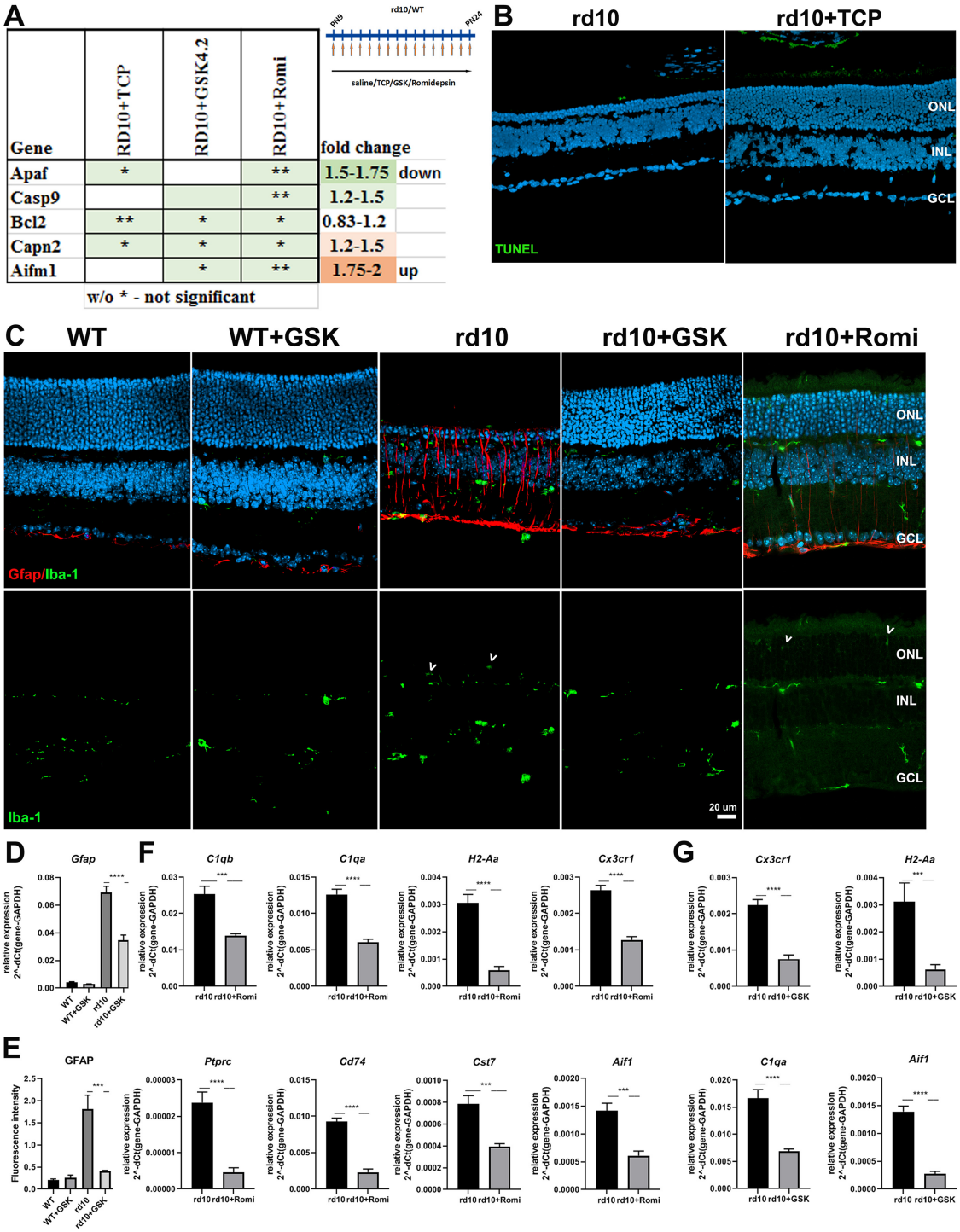

Figure 9. Treatment of rd10 with inhibitors specific for LSD1 and HDAC1 leads to decreased cell death, gliosis, and inflammation. ***A***, Heatmap of expression of cell death genes measured by RT-PCR for retinas P24 mice treated from P9 until P24 with inhibitors for LSD1 (TCP and GSK) and HDAC1 (romidepsin) compared with controls rd10 mice treated with saline only. The relative expression level for each gene was calculated by the 2-ΔΔCt method and normalized to GAPDH, with fold increase shown in orange or decrease shown in green. ***B***, Immunofluorescence microscopic images of retina sections from P24 WT mice treated from P9 until P24 with TCP or only saline (control), stained with TUNEL and nuclear counterstained with Hoechst33358. GCL, ganglion cell layer. ***C***, Immunofluorescence microscopic images of retina sections from P24 rd10 and WT mice treated from P9 until P24 with GSK, romidepsin, or only saline (control), stained with IBA1 (green, for *Aif1* gene), GFAP (red), and nuclear counterstained with Hoechst33358. GCL, ganglion cell layer. Scale bar, 20 μm White arrowheads indicate IBA1 positive microglia cells in ONL. ***D***, Comparison of gene expression levels for *Gfap* in mice at P24; WT and rd10 mice were treated with saline or with GSK from P9 until P24. ***E***, Image quantification of immunofluorescence intensity from ***C*** for GFAP for the rd10 and WT retinas treated with GSK or saline (control). ***F***, Comparison of gene expression levels for inflammatory markers in mice at P24; rd10 mice were treated with saline or with romidepsin from P9 until P24. ***G***, Comparison of gene expression levels for inflammatory markers in mice at P24; rd10 mice were treated with saline or with GSK from P9 until P24. In all cases, experiments were conducted with three to four biological and three technical replicates. *$p < 0.05$, **$p < 0.01$, ***$p < 0.001$, ****$p < 0.0001$ (±SEM).

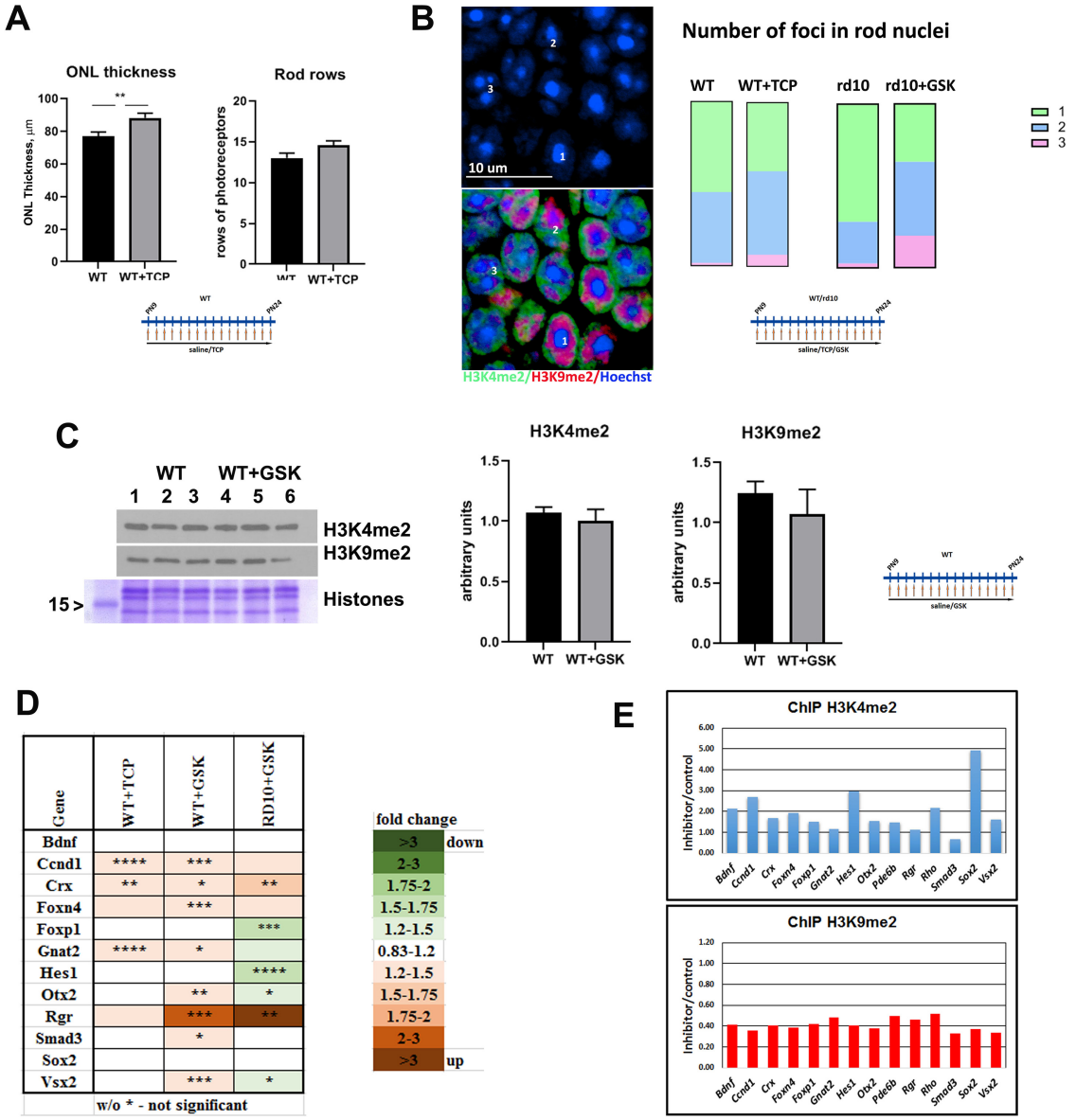

Figure 10. LSD1 inhibition promotes epigenetic changes that create more open and accessible chromatin in rod nuclei. ***A***, ONL thickness and rods rows were counted in central retina for P24 WT mice treated from P9 until P24 with TCP or only with saline for three to five biological and three technical replicas (±SEM). $^{**}p < 0.01$. ***B***, Comparison of the number of foci in rod nuclei in central retina at P24 for WT mice treated with saline or TCP and rd10 mice treated with saline or GSK from P9 until P24. Experiments were done for three to four biological and three technical replicas; 300–450 nuclei were counted for each sample. Left, Representative immunofluorescence microscopic image of rod photoreceptors in ONL in central mouse retina sections from P24 rd10 mice treated with GSK from P9 until P24. Bottom, Anti-H3K4me2 staining is in green (euchromatin), anti-H3K9me2 staining is in red (facultative heterochromatin), and nuclear counterstaining with Hoechst33358 is in blue (constitutive heterochromatin). Top, Image of only Hoechst33358 counterstaining demonstrates that rod photoreceptor nuclei have one, two, or three foci of heterochromatin. Right, Comparison of number of foci in rod nuclei in central retina at P24 for WT mice treated with saline or TCP and rd10 mice treated with saline or GSK from P9 until P24. Experiments were done for three to four biological and three technical replicas; 300–450 nuclei were counted for each sample. ***C***, Left, Anti-H3K4me2 and anti-H3K9me2 Western blot with samples of retina at P24 from WT mice treated with saline or with GSK from P9 until P24. Histone Coomassie staining was used as loading control. Right, Band intensity quantification was done for three biological and three technical replicates for anti-H3K4me2 and H3K9me2 Western. Intensity of bands for histone modifications were normalized on intensity for core histone Coomassie staining. ***D***, Heatmap of expression of progenitor/cell cycle genes measured by RT-PCR for retinas from P24 mice WT treated from P9 until P24 with inhibitors for LSD1 (TCP and GSK) relative to WT treated with saline and rd10 mice treated from P9 until P24 with GSK and compared with rd10 treated with saline. Each set of data represents three to five biological and three technical replicates (±SEM). The relative expression level for each gene was calculated by the 2-ΔΔCt method and normalized to GAPDH. $^{*}p < 0.05$, $^{**}p < 0.01$, $^{***}p < 0.001$, $^{****}p < 0.0001$ with fold increase in orange or decrease in green. ***E***, Comparison of H3K4me2 and H3K9me2 accumulation on gene regulatory elements such as promoter and enhancer in mice retina at P24; WT mice were treated with saline or GSK from P9 until P24. Quantitative PCRs were done with primers (Table 2) for the area around gene regulatory elements in three technical replicas.

10*B*), and an increase in the proportion of open and accessible chromatin. The morphologic changes in chromatin condensation we observed were supported by measurements of increased ONL thickness (Fig. 10*A*) and upregulated expression of progenitor/cell cycle genes (Fig. 10*D*). A cluster of upregulated genes belong to the Wnt pathway and have been shown to play a role in neuroprotection (Holly et al., 2014; Cisneros et al., 2020). The pleiotropic changes in gene expression induced by the epigenetic inhibitors support a change in cell state or metabolism that allows survival and function of rod photoreceptors without deleterious changes in other retinal cell types.

Susceptibility to cell death (and degeneration) or to reentry into the cell cycle (and malignant transformation) are inversely correlated, and the underlying mechanism determining these two opposite cellular properties is epigenome organization (Dyer, 2016). Cells with more open active chromatin organization can more easily survive change in cellular homeostasis in response to stress, but such cells are prone to cancerous transformation. Cells with a more closed heterochromatic nuclear organization are less susceptible to malignancy but have a lower ability to survive stress, making them predisposed to degeneration and cell death. Mature rod photoreceptors, like most neurons, belong to the second group of cells and have a uniquely closed chromatin organization (Solovei et al., 2009; Popova et al., 2013; Hughes et al., 2017). Our study shows that loosening or decondensing heterochromatin in rods can reduce degeneration and allow better survival of rod photoreceptors under stress conditions but, based on Ki67 labeling, do not demonstrate reentry into the cell cycle (data not shown).

The second molecular mechanism detected in rd10 was a dramatic decrease in inflammatory markers. We compared retina gene expression profiles by RNA-seq in rd10 versus WT (Fig. 4*C*) and demonstrated a dramatic upregulation of several inflammatory pathways (Fig. 4*E*,*G*; Table 3) that was reversed by treatment with LSD1 inhibitor GSK (Fig. 4*D*,*F*,*H*). LSD1 participates in a signaling cascade (PKCα - LSD1 - NF-kB) and demethylates one of the subunits of the NF-kB complex, p65 (gene *Rela*), enhancing its ability to activate expression of NF-kB target genes in the inflammatory response during sepsis (Kim et al., 2018) and colitis (Oh et al., 2020). We propose that a similar pathway is activated during retina degeneration and that LSD1 inhibition blocks this pathway and abrogates inflammation. Our findings support previous work that has suggested a role for immune responses in both mouse models of RP and in human patients (Gupta et al., 2003; Zhao et al., 2015; Zabel et al., 2016; O'Koren et al., 2019; Ronning et al., 2019; Wieghofer et al., 2021).

Interestingly, we found that HDAC1 inhibition has an inhibitory effect on transcription of inflammatory genes similar to LSD1 inhibition. Although LSD1and HDAC1 are known to interact synergistically in the nucleus to change patterns of epigenetic histone modifications, there is less evidence for such an interaction for nonhistone targets. Acetylation of p65 reduces its binding to DNA in promoter regions of inflammatory genes (Kiernan et al., 2003). Thus, HDAC inhibition with romidepsin could lead to higher acetylation of p65 and inhibition of transcription regulated by the NF-kB pathway. Further studies are needed to examine whether LSD1 and HDAC1 are working in a common complex or on common targets to regulate inflammatory response during neurodegeneration.

A number of previous studies have tested epigenetic modifiers as possible therapeutics for retinitis pigmentosa. Some of these have focused on the neuroprotective effects of blocking HDAC activity by such nonselective inhibitors as TSA, valproic acid (VPA), and sodium butyrate (Chuang et al., 2009; Zhang et al., 2015), all of which have some protective effect on RP (Mitton et al., 2014; Zhang et al., 2015; Berner and Kleinman, 2016; Todd and Zelinka, 2017; Vent-Schmidt et al., 2017). The broad-spectrum HDAC inhibitor VPA has been tested as a therapeutic agent for retinal degeneration with mixed results (Clemson et al., 2011; Kumar et al., 2014; Iraha et al., 2016; Totan et al., 2017). Recently, selective inhibitors that are specific for subclasses of HDACs were tested to prevent neurodegeneration; for example, the specific inhibition of HDAC3 by RGFP966 protected against RGC death in models of optic nerve injury (Schmitt et al., 2017).

Potential treatments with other modifiers that lessen chromatin compaction is just beginning. Inhibition of DNA methylation in rd1 mice with decitabine resulted in a reduction of photoreceptor loss (Farinelli et al., 2014). Inhibition of PRC2 deposition of the repressive chromatin mark H3K27me3 by DZNep led to delays in retinal degeneration in rd1 mice (Zheng et al., 2018). BMI1 is a component of another polycomb repressive complex 1 (PRC1) and also performs chromatin compaction by activating PRC2 complex. Knocking out BMI1 resulted in photoreceptor survival in rd1 retinas (Zencak et al., 2013). Pharmacological inhibition of HDAC11 and SUV39H2, which made chromatin more open and accessible, ameliorated age-related macular degeneration (Luu et al., 2020). Whether some or all of these compounds also inhibit inflammation is not known.

We tested the Class I HDAC inhibitor romidepsin that is approved for use in treating peripheral and cutaneous T-cell lymphoma. We found that romidepsin was moderately effective at preventing rod degeneration in rd10 mice and increased the levels of expression of mostly early rod genes but not photoreceptor TFs or later rod and cone genes, probably because it caused higher decondensation of chromatin than LSD1 inhibitors. Animals treated with romidepsin, however, showed poorer weight gain and were less active than those treated with other agents. Although intraocular or topical treatments with romidepsin or related compounds might overcome some of the systemic negative effects, our data suggest that there are better systemic treatments.

Our results clearly show that inhibiting LSD1 with either TCP or GSK led to increased survival of photoreceptors and no deleterious effects on other retinal cells, with decreased expression of markers of inflammation, cell death, and gliosis. Interestingly, the treatments were able to stop degeneration at whatever point they were started, but the degeneration resumed when the treatments ceased. The best result for retina preservation in rd10 mice was obtained with the specific LSD1 inhibitor GSK. Although a better response was detected with the higher dose used, we found that drug application every two days was just as effective and had fewer side effects in that animals showed more normal gains in body weight and were more active.

The heterogeneity of RP has hindered the development of general therapies. We have demonstrated that pharmacological manipulation of LSD1 and HDAC1 alters the epigenetic landscape in ways that lessen the impact of deleterious mutations and inflammation and allows extended survival of rod photoreceptors. Additional studies on other mouse models of RP are needed to show that treatment with an epigenetic inhibitor is mutation independent. Intraocular injection or topical application instead of systemic administration could help to eliminate side effects of drugs and should restrict epigenetic changes to the eye. With such targeted applications it will be possible to study the pharmacokinetic and bioactivity of epigenetic drugs to achieve the optimum neuroprotective effect.

We propose that epigenetic modifiers such as those used in this study can effectively treat RP because of their dual action. By reducing inflammation, they provide an environment in which a more open chromatin structure can allow usage of a wider array of homeostatic mechanisms to survive and prevent cell death pathway activation.

References

Adamo A, Sesé B, Boue S, Castaño J, Paramonov I, Barrero MJ, Izpisua Belmonte JC (2011) LSD1 regulates the balance between self-renewal and differentiation in human embryonic stem cells. Nat Cell Biol 13:652–659.

Aldiri I, Xu B, Wang L, Chen X, Hiler D, Griffiths L, Valentine M, Shirinifard A, Thiagarajan S, Sablauer A, Barabas M-E, Zhang J, Johnson D, Frase S, Zhou X, Easton J, Zhang J, Mardis ER, Wilson RK, Downing JR, et al. (2017) The dynamic epigenetic landscape of the retina during development, reprogramming, and tumorigenesis. Neuron 94:550–568. e10.

Arango-Gonzalez B, Trifunović D, Sahaboglu A, Kranz K, Michalakis S, Farinelli P, Koch S, Koch F, Cottet S, Janssen-Bienhold U, Dedek K, Biel M, Zrenner E, Euler T, Ekström P, Ueffing M, Paquet-Durand F (2014) Identification of a common non-apoptotic cell death mechanism in hereditary retinal degeneration. PLoS One 9:e112142.

Barnstable CJ (1980) Monoclonal antibodies which recognize different cell types in the rat retina. Nature 286:231–235.

Berner AK, Kleinman ME (2016) Therapeutic approaches to histone reprogramming in retinal degeneration. Adv Exp Med Biol 854:39–44.

Bishton MJ, Harrison SJ, Martin BP, McLaughlin N, James C, Josefsson EC, Henley KJ, Kile BT, Prince HM, Johnstone RW (2011) Deciphering the molecular and biologic processes that mediate histone deacetylase inhibitor-induced thrombocytopenia. Blood 117:3658–3668.

Candido EP, Reeves R, Davie JR (1978) Sodium butyrate inhibits histone deacetylation in cultured cells. Cell 14:105–113.

Chang B, Hawes NL, Hurd RE, Davisson MT, Nusinowitz S, Heckenlively JR (2002) Retinal degeneration mutants in the mouse. Vision Res 42:517–525.

Chang B, Hawes NL, Pardue MT, German AM, Hurd RE, Davisson MT, Nusinowitz S, Rengarajan K, Boyd AP, Sidney SS, Phillips MJ, Stewart RE, Chaudhury R, Nickerson JM, Heckenlively JR, Boatright JH (2007) Two mouse retinal degenerations caused by missense mutations in the beta-subunit of rod cGMP phosphodiesterase gene. Vision Res 47:624–633.

Charish J, Shabanzadeh AP, Chen D, Mehlen P, Sethuramanujam S, Harada H, Bonilha VL, Awatramani G, Bremner R, Monnier PP (2020) Neogenin neutralization prevents photoreceptor loss in inherited retinal degeneration. J Clin Invest 130:2054–2068.

Chuang DM, Leng Y, Marinova Z, Kim HJ, Chiu CT (2009) Multiple roles of HDAC inhibition in neurodegenerative conditions. Trends Neurosci 32:591–601.

Cisneros E, di Marco F, Rueda-Carrasco J, Lillo C, Pereyra G, Martín-Bermejo MJ, Vargas A, Sanchez R, Sandonís Á, Esteve P, Bovolenta P (2020) Sfrp1 deficiency makes retinal photoreceptors prone to degeneration. Sci Rep 10:5115.

Clemson CM, Tzekov R, Krebs M, Checchi JM, Bigelow C, Kaushal S (2011) Therapeutic potential of valproic acid for retinitis pigmentosa. Br J Ophthalmol 95:89–93.

Dyer MA (2016) Lessons from retinoblastoma: implications for cancer, development, evolution, and regenerative medicine. Trends Mol Med 22:863–876.

Farinelli P, Perera A, Arango-Gonzalez B, Trifunovic D, Wagner M, Carell T, Biel M, Zrenner E, Michalakis S, Paquet-Durand F, Ekström PA (2014) DNA methylation and differential gene regulation in photoreceptor cell death. Cell Death Dis 5:e1558.

Ferreira RC, Popova EY, James J, Briones MR, Zhang SS, Barnstable CJ (2017) Histone deacetylase 1 is essential for rod photoreceptor differentiation by regulating acetylation at histone H3 lysine 9 and histone H4 lysine 12 in the mouse retina. J Biol Chem 292:2422–2440.

Gargini C, Terzibasi E, Mazzoni F, Strettoi E (2007) Retinal organization in the retinal degeneration 10 (rd10) mutant mouse: a morphological and ERG study. J Comp Neurol 500:222–238.

Gupta N, Brown KE, Milam AH (2003) Activated microglia in human retinitis pigmentosa, late-onset retinal degeneration, and age-related macular degeneration. Exp Eye Res 76:463–471.

Hart AW, McKie L, Morgan JE, Gautier P, West K, Jackson IJ, Cross SH (2005) Genotype-phenotype correlation of mouse pde6b mutations. Invest Ophthalmol Vis Sci 46:3443–3450.

Holly VL, Widen SA, Famulski JK, Waskiewicz AJ (2014) Sfrp1a and Sfrp5 function as positive regulators of Wnt and BMP signaling during early retinal development. Dev Biol 388:192–204.

Hughes AE, Enright JM, Myers CA, Shen SQ, Corbo JC (2017) cell type-specific epigenomic analysis reveals a uniquely closed chromatin architecture in mouse rod photoreceptors. Sci Rep 7:43184.

Iraha S, Hirami Y, Ota S, Sunagawa GA, Mandai M, Tanihara H, Takahashi M, Kurimoto Y (2016) Efficacy of valproic acid for retinitis pigmentosa patients: a pilot study. Clin Ophthalmol 10:1375–1384.

Iribarne M, Masai I (2018) Do cGMP levels drive the speed of photoreceptor degeneration? Adv Exp Med Biol 1074:327–333.

Jain S, Jirau-Serrano X, Zullo KM, Scotto L, Palermo CF, Sastra SA, Olive KP, Cremers S, Thomas T, Wei Y, Zhang Y, Bhagat G, Amengual JE, Deng C, Karan C, Realubit R, Bates SE, O'Connor OA (2015) Preclinical pharmacologic evaluation of pralatrexate and romidepsin confirms potent synergy of the combination in a murine model of human T-cell lymphoma. Clin Cancer Res 21:2096–2106.

Kang S, Larbi D, Andrade M, Reardon S, Reh TA, Wohl SG (2020) A comparative analysis of reactive müller glia gene expression after light damage and microRNA-depleted Müller glia-focus on microRNAs. Front Cell Dev Biol 8:620459.

Kerenyi MA, Shao Z, Hsu YJ, Guo G, Luc S, O'Brien K, Fujiwara Y, Peng C, Nguyen M, Orkin SH (2013) Histone demethylase Lsd1 represses hematopoietic stem and progenitor cell signatures during blood cell maturation. Elife 2:e00633.

Kiernan R, Brès V, Ng RW, Coudart MP, El Messaoudi S, Sardet C, Jin DY, Emiliani S, Benkirane M (2003) Post-activation turn-off of NF-kappa B-dependent transcription is regulated by acetylation of p65. J Biol Chem 278:2758–2766.

Kim D, Nam HJ, Lee W, Yim HY, Ahn JY, Park SW, Shin HR, Yu R, Won KJ, Bae JS, Kim KI, Baek SH (2018) PKCα-LSD1-NF-κB-signaling cascade is crucial for epigenetic control of the inflammatory response. Mol Cell 69:398–411.e6.

Kumar A, Midha N, Gogia V, Gupta S, Sehra S, Chohan A (2014) Efficacy of oral valproic acid in patients with retinitis pigmentosa. J Ocul Pharmacol Ther 30:580–586.

Laurent B, Ruitu L, Murn J, Hempel K, Ferrao R, Xiang Y, Liu S, Garcia BA, Wu H, Wu F, Steen H, Shi Y (2015) A specific LSD1/KDM1A isoform regulates neuronal differentiation through H3K9 demethylation. Mol Cell 57:957–970.

Lobanova ES, Finkelstein S, Li J, Travis AM, Hao Y, Klingeborn M, Skiba NP, Deshaies RJ, Arshavsky VY (2018) Increased proteasomal activity supports photoreceptor survival in inherited retinal degeneration. Nat Commun 9:1738.

Luu J, Kallestad L, Hoang T, Lewandowski D, Dong Z, Blackshaw S, Palczewski K (2020) Epigenetic hallmarks of age-related macular degeneration are recapitulated in a photosensitive mouse model. Hum Mol Genet 29:2611–2624.

McLaughlin ME, Sandberg MA, Berson EL, Dryja TP (1993) Recessive mutations in the gene encoding the beta-subunit of rod phosphodiesterase in patients with retinitis pigmentosa. Nat Genet 4:130–134.

Mitton KP, Guzman AE, Deshpande M, Byrd D, DeLooff C, Mkoyan K, Zlojutro P, Wallace A, Metcalf B, Laux K, Sotzen J, Tran T (2014) Different effects of valproic acid on photoreceptor loss in Rd1 and Rd10 retinal degeneration mice. Mol Vis 20:1527–1544.

Mohammad HP, Smitheman KN, Kamat CD, Soong D, Federowicz KE, Van Aller GS, Schneck JL, Carson JD, Liu Y, Butticello M, Bonnette WG, Gorman SA, Degenhardt Y, Bai Y, McCabe MT, Pappalardi MB, Kasparec J, Tian X, McNulty KC, Rouse M, et al. (2015) A DNA hypomethylation signature predicts antitumor activity of LSD1 inhibitors in SCLC. Cancer Cell 28:57–69.

Murakami Y, Ishikawa K, Nakao S, Sonoda KH (2020) Innate immune response in retinal homeostasis and inflammatory disorders. Prog Retin Eye Res 74:100778.

Newton F, Megaw R (2020) Mechanisms of photoreceptor death in retinitis pigmentosa. Genes (Basel) 11:1120.

Norrie JL, Lupo MS, Xu B, Al Diri I, Valentine M, Putnam D, Griffiths L, Zhang J, Johnson D, Easton J, Shao Y, Honnell V, Frase S, Miller S, Stewart V, Zhou X, Chen X, Dyer MA (2019) Nucleome dynamics during retinal development. Neuron 104:512–528.e11.

O'Koren EG, Yu C, Klingeborn M, Wong AYW, Prigge CL, Mathew R, Kalnitsky J, Msallam RA, Silvin A, Kay JN, Bowes Rickman C, Arshavsky VY, Ginhoux F, Merad M, Saban DR (2019) Microglial function is distinct in different anatomical locations during retinal homeostasis and degeneration. Immunity 50:723–737.e7.

Oh C, Jeong J, Oh SK, Baek SH, Kim KI (2020) Inhibition of LSD1 phosphorylation alleviates colitis symptoms induced by dextran sulfate sodium. In. BMB Rep 53:385–390.

Popova EY, Pinzon-Guzman C, Salzberg AC, Zhang SS, Barnstable CJ (2016) LSD1-mediated demethylation of H3K4me2 is required for the transition from late progenitor to differentiated mouse rod photoreceptor. Mol Neurobiol 53:4563–4581.

Popova EY, Grigoryev SA, Fan Y, Skoultchi AI, Zhang SS, Barnstable CJ (2013) Developmentally regulated linker histone H1c promotes heterochromatin condensation and mediates structural integrity of rod photoreceptors in mouse retina. J Biol Chem 288:17895–17907.

Popova EY, Xu X, DeWan AT, Salzberg AC, Berg A, Hoh J, Zhang SS, Barnstable CJ (2012) Stage and gene specific signatures defined by histones H3K4me2 and H3K27me3 accompany mammalian retina maturation in vivo. PLoS One 7:e46867.

Power M, Das S, Schütze K, Marigo V, Ekström P, Paquet-Durand F (2020a) Cellular mechanisms of hereditary photoreceptor degeneration—Focus on cGMP. Prog Retin Eye Res 74:100772.

Power MJ, Rogerson LE, Schubert T, Berens P, Euler T, Paquet-Durand F (2020b) Systematic spatiotemporal mapping reveals divergent cell death pathways in three mouse models of hereditary retinal degeneration. J Comp Neurol 528:1113–1139.

Prusky GT, Alam NM, Beekman S, Douglas RM (2004) Rapid quantification of adult and developing mouse spatial vision using a virtual optomotor system. Invest Ophthalmol Vis Sci 45:4611–4616.

Riggs MG, Whittaker RG, Neumann JR, Ingram VM (1977) n-Butyrate causes histone modification in HeLa and Friend erythroleukaemia cells. Nature 268:462–464.

Ronning KE, Karlen SJ, Miller EB, Burns ME (2019) Molecular profiling of resident and infiltrating mononuclear phagocytes during rapid adult retinal degeneration using single-cell RNA sequencing. Sci Rep 9:4858.

Sancho-Pelluz J, Alavi MV, Sahaboglu A, Kustermann S, Farinelli P, Azadi S, van Veen T, Romero FJ, Paquet-Durand F, Ekström P (2010) Excessive HDAC activation is critical for neurodegeneration in the rd1 mouse. Cell Death Dis 1:e24.

Schmitt HM, Schlamp CL, Nickells RW (2017) Targeting hdac3 activity with rgfp966 protects against retinal ganglion cell nuclear atrophy and apoptosis after optic nerve injury. J Ocul Pharmacol Ther 34:260–273.

Shi L, Cui S, Engel JD, Tanabe O (2013) Lysine-specific demethylase 1 is a therapeutic target for fetal hemoglobin induction. Nat Med 19:291–294.

Shi YJ, Matson C, Lan F, Iwase S, Baba T, Shi Y (2005) Regulation of LSD1 histone demethylase activity by its associated factors. Mol Cell 19:857–864.

Solovei I, Kreysing M, Lanctôt C, Kösem S, Peichl L, Cremer T, Guck J, Joffe B (2009) Nuclear architecture of rod photoreceptor cells adapts to vision in mammalian evolution. Cell 137:356–368.

Sun G, Alzayady K, Stewart R, Ye P, Yang S, Li W, Shi Y (2010) Histone demethylase LSD1 regulates neural stem cell proliferation. Mol Cell Biol 30:1997–2005.

Tan L, Xing D, Daley N, Xie XS (2019) Three-dimensional genome structures of single sensory neurons in mouse visual and olfactory systems. Nat Struct Mol Biol 26:297–307.

Tiwari P, Sahay S, Pandey M, Qadri SS, Gupta KP (2015) Combinatorial chemopreventive effect of butyric acid, nicotinamide and calcium glucarate against the 7,12-dimethylbenz(a)anthracene induced mouse skin tumorigenesis attained by enhancing the induction of intrinsic apoptotic events. Chem Biol Interact 226:1–11.

Todd L, Zelinka C (2017) Valproic acid for a treatment of retinitis pigmentosa: reasons for optimism and caution. J Neurosci 37:5215–5217.

Totan Y, Güler E, Yüce A, Derviş ogulları MS (2017) The adverse effects of valproic acid on visual functions in the treatment of retinitis pigmentosa. Indian J Ophthalmol 65:984–988.

Trachsel-Moncho L, Benlloch-Navarro S, Fernández-Carbonell Á, Ramírez-Lamelas DT, Olivar T, Silvestre D, Poch E, Miranda M (2018) Oxidative stress and autophagy-related changes during retinal degeneration and development. Cell Death Dis 9:812.

Vent-Schmidt RYJ, Wen RH, Zong Z, Chiu CN, Tam BM, May CG, Moritz OL (2017) Opposing Effects of valproic acid treatment mediated by histone deacetylase inhibitor activity in four transgenic X. laevis models of retinitis pigmentosa. J Neurosci 37:1039–1054.

Wang T, Reingruber J, Woodruff ML, Majumder A, Camarena A, Artemyev NO, Fain GL, Chen J (2018) The PDE6 mutation in the rd10 retinal degeneration mouse model causes protein mislocalization and instability and promotes cell death through increased ion influx. J Biol Chem 293:15332–15346.

Whyte WA, Bilodeau S, Orlando DA, Hoke HA, Frampton GM, Foster CT, Cowley SM, Young RA (2012) Enhancer decommissioning by LSD1 during embryonic stem cell differentiation. Nature 482:221–225.

Wieghofer P, Hagemeyer N, Sankowski R, Schlecht A, Staszewski O, Amann L, Gruber M, Koch J, Hausmann A, Zhang P, Boneva S, Masuda T, Hilgendorf I, Goldmann T, Böttcher C, Priller J, Rossi FM, Lange C, Prinz M (2021) Mapping the origin and fate of myeloid cells in distinct compartments of the eye by single-cell profiling. Embo j 40:e105123.

Won J, Shi LY, Hicks W, Wang J, Hurd R, Naggert JK, Chang B, Nishina PM (2011) Mouse model resources for vision research. J Ophthalmol 2011:391384.

Yoshida N, Ikeda Y, Notomi S, Ishikawa K, Murakami Y, Hisatomi T, Enaida H, Ishibashi T (2013) Laboratory evidence of sustained chronic inflammatory reaction in retinitis pigmentosa. Ophthalmology 120:e5–12.

Zabel MK, Zhao L, Zhang Y, Gonzalez SR, Ma W, Wang X, Fariss RN, Wong WT (2016) Microglial phagocytosis and activation underlying photoreceptor degeneration is regulated by CX3CL1-CX3CR1 signaling in a mouse model of retinitis pigmentosa. Glia 64:1479–1491.

Zencak D, Schouwey K, Chen D, Ekström P, Tanger E, Bremner R, van Lohuizen M, Arsenijevic Y (2013) Retinal degeneration depends on Bmi1 function and reactivation of cell cycle proteins. Proc Natl Acad Sci U S A 110:E593–601.

Zhang H, Dai X, Qi Y, He Y, Du W, Pang JJ (2015) Histone deacetylases inhibitors in the treatment of retinal degenerative diseases: overview and perspectives. J Ophthalmol 2015:250812.

Zhao L, Zabel MK, Wang X, Ma W, Shah P, Fariss RN, Qian H, Parkhurst CN, Gan WB, Wong WT (2015) Microglial phagocytosis of living photoreceptors contributes to inherited retinal degeneration. EMBO Mol Med 7:1179–1197.

Zheng S, Xiao L, Liu Y, Wang Y, Cheng L, Zhang J, Yan N, Chen D (2018) DZNep inhibits H3K27me3 deposition and delays retinal degeneration in the rd1 mice. Cell Death Dis 9:310.